LANGMUIR Article
Cite This: Langmuir XXXX, XXX, XXX−XXX
pubs.acs.org/Langmuir

Detachment of Rough Colloids from Liquid−Liquid Interfaces

Michele Zanini,[†] Ivan Lesov,[‡] Emanuele Marini,[†] Chiao-Peng Hsu,[†] Claudia Marschelke,[§] Alla Synytska,[§] Svetoslav E. Anachkov,[‡] and Lucio Isa*[,†]

[†]Laboratory for Interfaces, Soft Matter and Assembly, Department of Materials, ETH Zurich, Vladimir-Prelog Weg 5, 8093 Zürich, Switzerland

[‡]Department of Chemical and Pharmaceutical Engineering, Faculty of Chemistry and Pharmacy, Sofia University, 1 James Bourchier Avenue, 1164 Sofia, Bulgaria

[§]Department of Polymer Interfaces, Leibniz Institute of Polymer Research, Hohe Strasse 6, D-01069 Dresden, Germany

Supporting Information

ABSTRACT: Particle surface roughness and chemistry play a pivotal role in the design of new particle-based materials. Although the adsorption of rough particles has been studied in the literature, desorption of such particles remains poorly understood. In this work, we specifically focus on the detachment of rough and chemically modified raspberry-like microparticles from water/oil interfaces using colloidal-probe atomic force microscopy. We observe different contact-line dynamics occurring upon particle detachment (pinning vs sliding), depending on both the particle roughness and surface modification. In general, surface roughness leads to a reduction of the desorption force of hydrophobic particles into the oil and provides a multitude of pinning points that can be accessed by applying different loads. Our results hence suggest future strategies for stabilization and destabilization of Pickering emulsions and foams.

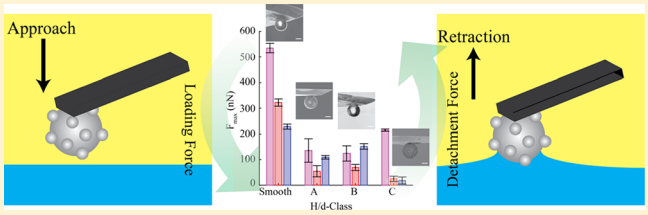

INTRODUCTION

Wetting is a phenomenon ubiquitous in nature and in industrial applications, typically associated with the spreading of a liquid onto a macroscopic solid surface. Young's law[1] describes the mechanical equilibrium of the surface tensions acting on a droplet, which defines its equilibrium shape and contact angle θ. The latter quantity is directly connected to the adhesion energy of the liquid onto the solid, where lower contact angles indicate favorable wetting. When a liquid spreads on a heterogeneous surface, for example, displaying surface roughness and/or chemical heterogeneity, contact angle hysteresis may occur. The droplet shape goes through out-of-equilibrium states originating from contact-line pinning at surface heterogeneities. As a result, the measured contact angle differs upon spreading or retracting the droplet, thus exhibiting distinct advancing and receding wetting angles,[2] respectively. Additionally, surface roughness alone is known to affect wetting, effectively making hydrophilic surfaces more hydrophilic and hydrophobic ones more hydrophobic.[3] If the solid surface is modified in terms of both texture and surface chemistry, a droplet can transition to the Cassie−Baxter[4] (CB) wetting regime, where a cushion of another fluid prevents the full contact between the droplet and the underlying surface. In such a case, solid surfaces can become superhydrophobic[5−7] and even superamphiphobic.[8−10] Rational design principles for a robust CB state have been studied both via experiments[11] and simulations,[12] showing that the transition between the suspended (CB) state to a fully wetting (Wenzel) state starts with the depinning of the contact line from the surface corrugations.

The same principles applied to macroscopic surfaces are implicitly translated to solid particles trapped at a liquid−fluid (e.g., water/air or water/oil) interface.[13,14] In this case, the contact angle determines the particle's adhesion energy and its relative position with respect to the interface. Contact-line pinning was also observed to impart a very large contact angle hysteresis at the single-particle level,[15] which can be exploited to devise design rules for particle-based emulsifiers.[15−18]

Depending on the size and nature of the particle surface heterogeneities, pinning and depinning of the contact line may or may not be thermally activated. In the former case, for nanometric chemical "defects," both slow relaxation of the contact line upon adsorption[19,20] and an increased viscous drag at the interface[21] have been reported. Conversely, surface asperities in the tens-of-nanometer range or above, even with uniform surface chemistry, lead to adsorbing particles that are trapped into very long-lived metastable states. This phenomenon originates from the fact that the energy associated with the dewetting of an individual asperity, required for contact line motion, greatly exceeds the thermal energy.[15] The absence of a spontaneous contact-angle evolution presents interesting possibilities to tune the wetting of rough particles after

Received: January 30, 2018
Revised: March 16, 2018
Published: March 29, 2018

DOI: 10.1021/acs.langmuir.8b00327
Langmuir XXXX, XXX, XXX−XXX

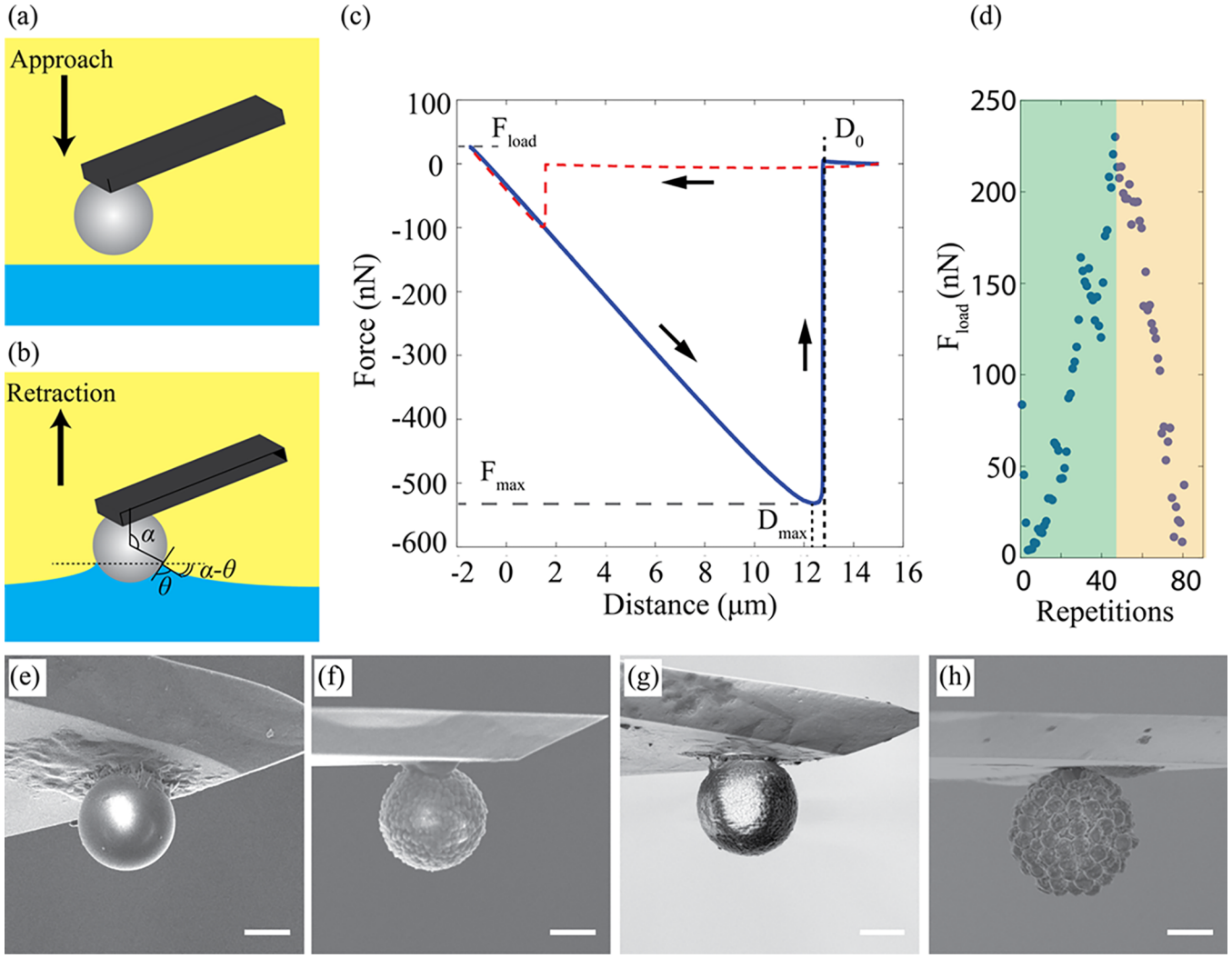

Figure 1. Schematic representations of the approach (a) and retraction (b) phases in a force measurement with colloidal-probe AFM at liquid−liquid interfaces. In (b), the contact angle θ and the central angle α are highlighted. (c) Example of an AFM force−distance curve obtained for a colloidal probe at a liquid−liquid interface. The dashed red line represents the approach of a smooth colloid to the liquid−liquid interface, whereas the blue line describes the retraction part. The maximal load exerted on the interface during the approach is labeled as F_{load}. F_{max} is the maximal adhesion force between the colloidal probe and the interface. D_{max} is the distance that corresponds to F_{max}. D_0 indicates the maximal detachment distance. (d) The approach−retraction curves are repeated many times by changing the applied load using the shown force-ramp profile. The green area corresponds to an increase in the load, whereas in the second part (orange), F_{load} gradually decreases. (e−h) SEM micrographs of smooth and rough silica colloidal probes used for the force−distance experiments. The images correspond to typical probes with $\langle H\rangle/\langle d\rangle$ values of ≈0, 0.39, 0.43, and 0.79, respectively. The scale bars correspond to 3 μm.

adsorption, and to devise very effective emulsion-stabilization strategies.[15−18,22,23]

In addition to affecting particle adsorption, the tuning and engineering of particle surface roughness also offers new angles to investigate the phenomenon of particle desorption from a fluid interface.[24] Desorption bears fundamental and applied relevance for many processes, including oil recovery, particle recycling, and froth floatation.[25,26] Nevertheless, in comparison to studies dealing with adsorption, systematic investigations of particle detachment phenomena are far less common.

For this reason, our study specifically focuses on the detachment of rough and chemically modified microparticles from liquid−liquid interfaces to shed light on the role of surface roughness on particle dewetting. To achieve our goal, we selected colloidal-probe atomic force microscopy (AFM) as the most suitable experimental method.

Since its invention, colloidal-probe AFM has been used to investigate the interactions between solid particles and a variety of soft and deformable interfaces, such as air bubbles,[27−32] water droplets,[29−31,33] and water/oil interfaces.[33−36] In particular, this technique allows for the direct measurement of the capillary force acting between a single particle and the fluid interface, both in advancing and in receding modes.

In mechanical equilibrium, spherical particles, which are small (negligible gravity), smooth, and chemically homogeneous, do not deform the interface in the vertical direction. In other words, the net capillary force at equilibrium is zero. By pulling the particle upward or pushing it downward, the interface deforms and a nonzero capillary force F arises.[24] Because the system is axially symmetric, the net capillary force F acting on the colloid has a vertical component only.

$$F = 2\pi R\gamma \sin(\alpha) \sin(\theta - \alpha) \quad (1)$$

DOI: 10.1021/acs.langmuir.8b00327
Langmuir XXXX, XXX, XXX−XXX

where R is the particle radius, γ is the interfacial tension, θ is the three-phase contact angle, and α is the central angle defining the position of the contact line on the particle surface.

In a typical experiment, such as the one sketched in Figure 1, a colloidal particle is attached onto a tipless AFM cantilever and brought into contact with the fluid interface. In this way, the interaction between the colloidal probe and the liquid interface can be measured by monitoring the vertical deflection of the cantilever. The latter is then translated into a force upon calibration. As a result, we obtain the force experienced by the probe as a function of its position, that is, a force−distance curve, where the position is finely controlled by means of a piezo actuator. Adsorption−desorption experiments repeated at different applied loads, that is, the maximum force with which the colloid is pressed onto the interface, allow investigating its effect on the maximal adhesion force, and, at the same time, ensure the robustness and reproducibility of the measurements. During the approach, as soon as the colloid interacts with the interface, it jumps into contact (assuming negligible repulsive interactions) and the distance covered by the piezo to restore a zero force is called the "jump-in distance." If the cantilever approaches a water surface, the jump-in distance can be used to measure the advancing contact angle.[27−29,32] Importantly, the point of zero force upon approach may or may not coincide with the particle equilibrium position, depending on the particle surface properties (i.e., the contact angle hysteresis).[36] The applied force is then increased to its maximum value F_{load}, followed by retraction at the same rate. While the piezo retracts, the absolute value of the detected force increases up to the maximum adhesion force F_{max}, until the particle snaps off (detaches) and the force goes back to zero. Hereafter, we exclusively focus on slow particle detachments from the interface with a continuous vertical displacement. The experiments are therefore to be considered quasi-static and displacement-controlled.[36]

There are two regimes of contact-line motion over the particle surface during detachment. First, the contact line can freely slide on the particle surface (sliding): the contact angle θ remains constant during the detachment process and α varies accordingly. Second, the contact line is fixed (pinning): the contact angle θ varies upon pulling, while the central angle α remains constant. In the particular case of contact-line pinning at a sharp edge, the contact angle can take a range of values described by Gibbs' inequality.[37]

For a displacement-controlled detachment, where the contact line can smoothly slide on the particle surface, the maximum value of the capillary force is achieved for $\alpha = (\pi + \theta)/2$[38,39]

$$F_{max} = 2\pi R\gamma \cos^2 \frac{\theta}{2} \quad (2)$$

Here, the distance travelled by the colloid's center of mass corresponding to F_{max} is labeled as D_{max} (see Figure 1). In analogy to the maximum detachment force, a maximum detachment distance D_0 can also be defined. In a conventional displacement-controlled experiment, D_0 is the maximal detachment distance, that is, the distance covered by the particle center of mass from the equilibrium position (point of zero force) to the point of particle detachment (see Figure 1). Upon further retraction beyond D_{max}, the measured force decreases (in absolute value), albeit in a different fashion depending on the contact-line motion modality. As an example of a system exhibiting contact-line pinning, Ally and co-workers[40] measured how a colloidal probe with a sharp cut, sculpted with a focused ion beam (FIB), adsorbed at the air/water interface. Contact-line pinning was always observed at the FIB cut, which was reached upon jump-in, and the adhesion force for the FIB-cut colloids differed from the value measured for regular particles with the same surface chemistry. In a complementary set of measurements, Anachkov and co-authors[36] carried out retraction experiments using smooth silica spheres with various surface chemistries at both air/water and oil/water interfaces. They demonstrated that the detachment proceeded via sliding of the contact line, and the force−distance curve could be described with only one input parameter, for example, F_{max} or D_0. If the contact line slides, the detachment is a gradual process, with a smooth decrease of F beyond F_{max} until D_0 is reached (see the example shown in Figure 1c). As a consequence, D_0 and D_{max} do not coincide. Conversely, for contact-line pinning, the detachment is very abrupt, and the values of D_0 and D_{max} practically coincide.

In this work, we explore further the interplay between particle detachment and surface properties, with the aim to achieve a deeper understanding of the different contact-line dynamics occurring upon particle detachment. The article is structured as follows. We first introduce the synthetic approach for the fabrication of rough particles, later used as AFM colloidal probes, as well as the methods applied to characterize their roughness. We then explain how the different surface functionalizations combined with the particle roughness affect the wetting of micron-sized colloids. In particular, we focus on the characteristic differences in the detachment behavior dictated by the regimes of contact-line motion: sliding versus pinning. In conclusion, we discuss the technological implications linked to the two possible detachment scenarios.

EXPERIMENTAL SECTION

Materials. Rough all-silica microparticles were fabricated as reported elsewhere[15,41] and as briefly described below. As smooth particles, we used monodisperse silica spheres with diameters of 6.27 ± 0.23 μm (microParticles GmbH, Germany). To obtain an AFM colloidal probe, both smooth and rough particles were immobilized on tipless cantilevers; see details below. To explore different degrees of hydrophobicity, the particles' surface chemistry was modified. In particular, we hydrophobized the colloidal probes using 1*H*,1*H*,2*H*,2*H*-perfluorooctyltriethoxysilane (98%, Sigma-Aldrich), octadecyltrichlorosilane (OTS, 95%, abcr GmbH), and α-bromo-isobutyryl bromide (BrIn, 98%, Aldrich). The interface was created using Milli-Q water and *n*-hexadecane (>99%, Sigma-Aldrich). The latter was purified from surface-active contaminants using a combination of alumina (MP EcoChrome Alumina B, Activity: Super I; MP Biomedicals) and silica (60 Å pores, 70−230 mesh, Fluka) columns. The equilibrium interfacial tension of the purified alkane against water was measured at room temperature by the pendant drop method (DSA100, KRÜSS GmbH) and had a value of 53.0 ± 0.5 mN/m. Ethanol (≥99.8%, Fluka) was used for rinsing the AFM cantilevers and the silicon wafers that were used as flat references.

Additional surface modifications were carried out using poly-(2,3,4,5,6-pentafluorostyrene) (PPFS, Aldrich, 99%), ethyl-α-bromo-isobutyrate (EBiB, Aldrich, 98%), copper(II) bromide (Aldrich, 99.999%), tin(II) 2-ethylhexanoate (Aldrich, 95%), α,α,α-trifluorotoluene (Sigma-Aldrich, ≥99%), tetrahydrofurane (Acros Organics, 99.99%), *N*,*N*,*N*′,*N*″,*N*″-pentamethyldiethylenetriamine (PMDTA, Aldrich, 99%), *N*,*N*-dimethylformamide (DMF, Aldrich, 99.8%), and anhydrous decalin (decahydronaphthalene ≥ 99%, mix cis + trans, anhydrous, Sigma-Aldrich).

Fabrication of All-Silica Rough Colloidal Probes. To fabricate model rough all-silica particles, we followed a synthesis strategy proposed in previous works.[15,41] This approach is based on the electrostatically driven heteroaggregation[42−45] of smaller silica particles

DOI: 10.1021/acs.langmuir.8b00327
Langmuir XXXX, XXX, XXX−XXX

("berries") onto larger silica colloids ("cores"), followed by surface roughness tailoring via heterogeneous nucleation of silica layers.[46]

In a typical procedure, 20 mg of 6.27 μm silica core particles were positively modified in 6 mL of 6.6 wt % aqueous solution of polydiallyldimethylammonium chloride (400−500 kDa, 20 wt %, Sigma-Aldrich), washed several times to remove the excess of unbound polyelectrolyte, and then decorated with 72 nm silica particles (72 ± 6 nm, Klebosol, Clariant) or with homemade silica particles with an average hydrodynamic diameter of 250 nm (polydisperse) or 960 nm (960 ± 36 nm) for at least 30 min under vigorous stirring. The suspensions were then washed several times to remove the excess of unadsorbed berries. The number of injected berries was estimated by assuming that they form a closely packed monolayer onto the geometrical equivalent of the cores' surface area. In this way, the smaller colloids were always in excess, so as to guarantee a more uniform surface coverage. When 960 nm berries were used, after their adsorption, 39 nm silica particles (39 ± 4 nm, Klebosol, Clariant) were also added to the suspension. The second population of berries can adsorb both on the primary (960 nm) asperities, forming a hierarchical structure, and into the available interstitial positions between the larger bumps, filling the gaps between them. This extra step is necessary to increase the overall surface area of the particles and therefore to ensure enhanced uniformity during the growth of the smoothing layer. The so-produced particles are termed native raspberry-like particles. To tune their surface roughness, a layer of silica was heteronucleated on the colloids' surface by means of a modified Stöber process.[46] In a typical reaction, 5 vol % tetraethyl orthosilicate (TEOS) solution in EtOH was dropped in a mixture of EtOH/NH_4OH/H_2O (77:13:10 vol %, 9.66 mL) containing 10 mg of native raspberry-like particles. The injected volumes of TEOS solution are reported in the Supporting Information (see Table S1). The selected injection rate was 0.1−0.3 mL/h. To suppress the formation of clusters during the smoothening process, the reaction was carried out under continuous ultrasonication. The smoothened rough colloids were then washed to remove possible nanoparticles formed by undesired homonucleation and then dried on a clean silicon wafer to be used as AFM colloidal probes.

Surface Roughness Characterization. The surface roughness of the produced raspberry-like particles was measured by scanning individual particles within a dried monolayer with an AFM (JPK NanoWizard 3, JPK). To make it possible, the rough particles were immobilized on a hydrophilized glass coverslip, following the preparation of a colloidal monolayer by convective assembly.[47] The AFM scans were performed with silicon nitride cantilevers (OMCL-AC160TS-OLYMPUS Micro Cantilevers, Japan) having a nominal spring constant of around 40 N/m and a resonance frequency of around 300 kHz in air under ambient conditions.

To decouple the topographical signal of interest (due to the berries) from the underlying particle curvature (due to the core), a custom-coded algorithm based on a least-squares approach was used.[15] The obtained background-free rough surface was then analyzed to extract the desired topographical information. In particular, the average asperity height $\langle H \rangle$ and the average asperity-to-asperity distance $\langle d \rangle$ were calculated. To extract $\langle d \rangle$, the asperities' centers of mass were detected, and then, the peak-to-peak distances were calculated using a Delaunay triangulation. In the case of the roughest particles (Figure 1h), scanning electron microscopy (SEM) image analysis was also used to give an estimate of $\langle H \rangle$ and $\langle d \rangle$. Because the distances obtained from the SEM micrographs are not curvature-free, only asperities close to the top of the colloid were considered to minimize the errors. Furthermore, in this case, $\langle H \rangle$ was assumed to coincide with the size of the "berries" measured in the SEM.

The particles were classified based on the values of the dimensionless roughness parameter $\langle H \rangle / \langle d \rangle$. This ratio takes into account both the number of asperities per unit length and their height, and it is therefore related to the probability for contact-line pinning at an asperity. The direct comparison between different roughness classes holds only if the shape of the asperities is consistent among those classes. The qualitative impression that the roughness features consist of spherical caps was proven by the quantitative three-dimensional (3D) reconstruction and analysis of individual asperities (Figure S1). Given the spherical shape of the roughness features, it is possible to apply both the estimate provided by Zanini and co-workers[15] for the energy for dewetting of an individual asperity and the approach used by Ye and co-authors[48] to describe the impalement of a rough colloid; see the details in the Results and Discussion section. The classical description of the surface topography via root-mean-square (rms) roughness is reported in the Supporting Information (Figure S2).

Hydrophobization Procedure by Vapor Deposition. Some colloidal probes were surface-modified by silanization using vapor deposition of 1*H*,1*H*,2*H*,2*H*-perfluorooctyltriethoxysilane (hereafter, fluorosilane) and OTS. The silica surface of the colloidal probes, glued on the cantilevers, was initially hydrophilized and activated in an ultraviolet (UV)−ozone chamber (Boekel UV cleaner, model 135500, Boekel Industries Inc.) for at least 10 min. In this way, a uniform layer of silanol groups was created on the particles' surface, enhancing the homogeneity and efficiency of the subsequent silanization step. Next, the samples were hydrophobized in the presence of silane vapors for at least 90 min at room temperature. Smooth, flat, silicon wafers with a silica layer on top were modified at the same time using the same procedure and were used as references.

Hydrophobization in Solution. Surface hydrophobization was also carried out in solution. For the bromo-modified colloidal probes, we adapted an existing protocol.[15,49] The silica surface of the colloidal probes, glued on the cantilevers, was activated in a UV−ozone chamber for at least 10 min. Next, the particles were modified in the presence of 3-aminopropyltriethoxysilane (APTES, 99%, Acros Organics) vapors to introduce amino groups to the surface. The APTES-modified colloidal probes were degassed with nitrogen [N_2(g)] for at least 10 min, immersed in dry dichloromethane (20 mL), and then exposed to distilled trimethylamine (1.6 mL) and BrIn (0.8 mL, 6.4 mM) at room temperature for 4 h. In this way, BrIn could graft onto the aminosilane-coated surfaces, providing the desired bromo-functionalization. The samples were then rinsed in fresh dichloromethane and dried in air. Smooth, flat, silicon wafers with a silica layer on top were modified at the same time using the same procedure and were used as references.

Additional measurements were carried out to investigate the role of possible contact-line pinning coming from surface chemical heterogeneities. In this case, the silica colloids were hydrophobized in solution by means of both OTS and poly(pentafluorostyrene) brushes. The so-modified colloids were exclusively used for interfacial deformation studies. OTS was applied to the surface, as already reported in the literature.[15,50] Briefly, silica particles (10 mg) were dried overnight, redispersed in 5 mL of anhydrous decalin (decahydronaphthalene, mix cis + trans, anhydrous, Sigma-Aldrich), and modified at 25 °C in the presence of 30 μL of OTS for 4 h. Purification was carried out by several centrifugation/redispersion steps in decalin and ethanol.

PPFS was grafted via surface-initiated atom transfer radical polymerization[51] using the particles modified with BrIn as follows: 4 mL of PPFS, 100 μL of PMDTA (0.5 M solution in DMF), 100 μL of $CuBr_2$ (0.1 M solution in DMF), and 0.15 μL of EBiB were added to the particles (50 mg). The mixture was sonicated and purged with Ar, followed by the injection of 300 μL of tin(II)-2-ethylhexanoate. Polymerization was performed under continuous stirring at 80 °C in an oil bath for 30 min. Subsequently, the particles with the grafted polymer were washed several times in α,α,α-trifluorotoluene, then in ethanol, and finally dried under vacuum at 25 °C. This procedure was preferred to vapor modification (see above) to achieve a uniform surface modification, so that we could study the adsorption of free colloids, that is, not attached to a cantilever [see Gel-Trapping Technique (GTT) section].

Colloidal-Probe AFM at Liquid−Liquid Interfaces. The capillary force acting on a silica microparticle trapped at the *n*-hexadecane/water interface was measured with an AFM (JPK NanoWizard 3, JPK, Germany). The experiments were carried out following procedures already reported in the literature.[27,28,33,36] Individual colloids were attached to tipless cantilevers (spring constant ranging from ∼28 to 70 N/m, All-In-One-Al-TL; BudgetSensors)

DOI: 10.1021/acs.langmuir.8b00327
Langmuir XXXX, XXX, XXX−XXX

using a micromanipulator and UV-curable glue (Norland Optical Adhesive 61, Norland Products Inc.). Every colloidal probe was imaged with SEM (LEO1530, Zeiss) before any further use. Prior to SEM imaging, the colloids were not sputtered with any conductive layer. As a result of the SEM imaging, the colloidal probes presenting defects, for example, glue excesses, were detected and excluded. To minimize the thermal drift of the cantilever during measurements, the colloidal probes were fully immersed into *n*-hexadecane, and the laser was turned on for at least 30 min before the experiments started.[36] Once thermally equilibrated, the cantilevers were calibrated using the thermal noise method.[52] The optical detector sensitivity was determined by taking a force curve on a rigid surface immersed in *n*-hexadecane before each measurement set. All force measurements were conducted in a homemade liquid cell,[36] which consisted of a truncated metal cone (1.5 mm height and 2 mm diameter of the truncated upper part) glued on a Petri dish (25 mm in diameter). Before each measurement, the cone was filled with fresh Milli-Q water and then covered with *n*-hexadecane. In all experiments, the interface was practically flat, and no curvature effects were considered. The interface was then centered below the colloidal probe by means of an optical microscope, and its vertical position was located by detecting the engagement of the probe in the force-controlled mode with a threshold value of 30 nN. The cantilever was then retracted by 15 μm (the maximal extension of the piezo actuator), and the automatic attachment−detachment cycles were initiated. Because the experiments were fully displacement-controlled, to increase (decrease) the load, the cantilever was moved toward (away from) the interface. Coarse adjustments were carried out with the stepper motors, whereas the fine-tuning was done by the piezo extension. For this reason, the indentation speed varied between 2.8 and 3 μm/s (the indentation time was set constant). All experiments were carried out at room temperature (25 °C).

For each measurement, multiple attachment−detachment repetitions were recorded, in which the loading force was varied systematically, resulting in a symmetric force-ramp profile (Figure 1d). The loading force F_{load} is defined as the maximum positive force used to deform the interface. An accurate determination of F_{max} from the raw force−distance data can be difficult at times because of oscillations around the force minimum. To avoid this issue, the force−distance curves were mathematically smoothed to remove spurious oscillations, if any. In particular, the number of data points in each curve (n) was divided by the actual length of the retraction curve (L) in nm, and thus, we obtained the spatial resolution (n/L) of the experiment. We then applied a moving-average (smoothing) procedure, where the number of averaged data points corresponded to the radius of the smallest asperity multiplied by the spatial resolution n/L. In this way, any oscillations that appeared over $36 \times n/L$ data points were averaged (neglected), hence removing high-frequency instrumental noise. F_{max} was then defined as the maximum (in terms of absolute value) of the noise-free retraction forces. This approach was used for all curves and all roughness classes. A second smoothing procedure was later applied to construct a baseline, relative to which the force oscillations were measured. In this case, the baseline was calculated by averaging over every $960 \times n/L$ data points, where 960 nm is the size of the biggest asperities. To avoid numerical artifacts in the baseline detection, the second smoothing procedure was used for all roughness classes.

Macroscopic Contact Angle Measurements. Static and dynamic contact angle measurements of droplets on chemically modified silicon wafers (mimicking the respective particle modifications) were performed by the sessile drop method using the drop-shape analysis technique (DSA100, KRÜSS, Germany). These measurements served as a reference to validate the quality of the surface modification and to provide a macroscopic and well-established standard. Milli-Q water or *n*-hexadecane (1−3 μL) was placed onto the silicon wafers modified with the procedures described above. The contact angles of the water droplets were determined on wafers immersed in *n*-hexadecane. The contact angle measurements with the *n*-hexadecane droplets were carried out in air. For advancing and receding contact angle measurements, a 5 μL droplet was expanded and retracted, respectively, onto the sample surface at a flow rate of 0.25 μL/s.

Gel-Trapping-Technique. A modified version of the GTT[21,53] was used to characterize the interfacial deformations around isolated OTS-coated and fluorinated colloids.[15] Here, we used the as-received gellan gum (AppliChem) to produce a 2 wt % aqueous mixture that was poured at 70 °C in clean Petri dishes, covered with hot *n*-hexadecane, and allowed to equilibrate for a few minutes. The particles of interest were previously dispersed in hot *n*-hexadecane, successively injected in the oil phase, and allowed to sediment at the interface. The samples were slowly cooled down to room temperature allowing for a uniform interfacial gelation. Next, the nonpolar (oil) phase was removed and substituted with UV-curable glue (Norland NOA63), which was then polymerized and used as a high-fidelity replica of the interface.[15]

To analyze the interfacial deformations, isolated colloids were imaged using AFM in tapping mode along two orthogonal directions. Both the trace and retrace signals were used for the analysis of the interfacial deformations. In this way, the same region of interest was imaged four times. The AFM scans were corrected for thermal drift and overlaid to enhance the signal-to-noise ratio. An edge-detection code based on Canny[54] and Sobel[55] methods was written to identify the three-phase contact line. For a more accurate detection, either the phase or the error signals of the AFM were used. The coordinates of the edge corresponded to the location of the contact line and served as reference points for the 3D reconstruction of the interface around the adsorbed colloids. To study the radial decay of the interfacial deformations, we fitted the height profile at a fixed polar angle φ with the expression

$$h(l) = A_0 + A_2 \times (R_c/l)^2 \tag{3}$$

In eq 3, R_c is the radius of the contact line, l is the radial distance from the particle center of mass, and A_0 and A_2 are the fitting parameters. For $l > R_c$, A_0 represents an offset in the experimental position of the interface, whereas A_2 indicates the amplitude of the quadrupolar deformation.[56,57] The experimental data were weighted as $\sqrt{l}$ to guarantee that the far-field deformations were correctly captured in the fit.

RESULTS AND DISCUSSION

Roughness Characterization. As previously reported,[15,41,58] the atomic force microscope is a precious analytical tool to investigate the surface topography of micron-sized particles. From the curvature-free height signal, roughness parameters can be extracted. In particular, one can locate the centers of the spherical asperities (crosses in Figure 2a) and measure their heights H (Figure 2b). From the asperities' positions, we calculated the distribution of the nearest peak-to-peak distance d (Figure 2c). We then decided to categorize our particles into roughness classes based on the dimensionless roughness parameter $\langle H\rangle/\langle d\rangle$, where $\langle H\rangle$ and $\langle d\rangle$ are the mean values of H and d, respectively. This ratio is proportional to the number of asperities per unit length[48] and is also connected to the probability for a three-phase contact line of length $\langle d\rangle$ to pin at a spherical asperity with height $\langle H\rangle$. The rough particles that we produced in this study give rise to $\langle H\rangle/\langle d\rangle$ values of 0.39 (RB_0.39), 0.43 (RB_0.43), and 0.79 (RB_0.79). Hereafter, the various roughness classes are denoted as "RB_$\langle H\rangle/\langle d\rangle$." Interestingly, RB_0.39 and RB_0.43 are characterized by very similar $\langle H\rangle/\langle d\rangle$ values, although their rms roughness values are markedly different (see the Supporting Information section 2 and Figure S2). Smooth particles have a value of $\langle H\rangle/\langle d\rangle \approx 0$.

Surface Functionalization. To validate the consistency and reproducibility of the chemical modification procedures, we compared the results obtained for smooth and flat silicon

DOI: 10.1021/acs.langmuir.8b00327
Langmuir XXXX, XXX, XXX−XXX

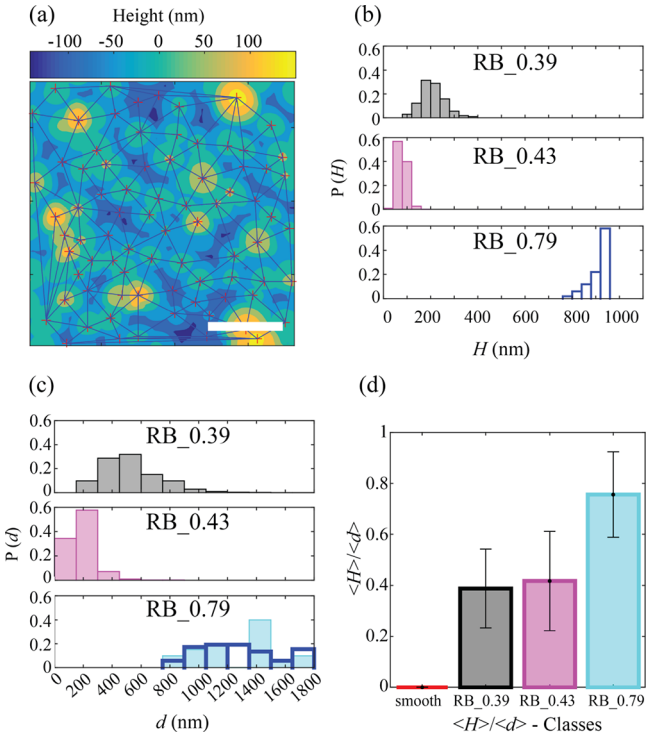

Figure 2. Roughness extraction for model micron-sized rough particles. (a) Background-free contour plot of the surface of a rough particle (from RB_0.39). The centers of each asperity and the triangulation used to calculate the asperity-to-asperity distance are highlighted. The scale bar is 500 nm. (b,c) Probability distributions of the asperity height H and the nearest inter-asperity distance d for all roughness classes, respectively. (d) Mean values of H/d corresponding to the distributions in (b,c) (in black—RB_0.39; in magenta—RB_0.43; in cyan—RB_0.79). All data, apart from the empty blue histograms in panel (b,c), are extracted from the AFM measurements. The empty histograms in (b,c) are extracted from the SEM image analysis.

surfaces with the single-particle data extracted for smooth colloidal probes. It is important to point out that the AFM piezo actuator used in the current work has a maximal extension of 15 μm. Consequently, large and hydrophilic colloids, which detach at distances D_0 larger than 15 μm, cannot be measured automatically. In these cases, the retraction is carried out manually by means of the AFM stepper motors,[36,48] and both the statistics and the accuracy of the measurements are compromised. Therefore, we chose to modify the surface of our rough particles to render them sufficiently hydrophobic, so that we can work within the piezo range. We performed three different kinds of hydrophobization: coating the particles with Br-silanes, OTS, and fluorosilanes, as described in detail in the Experimental Section. In Table 1, we compare the macroscopic contact angles of water droplets, measured on the modified silicon wafers immersed in *n*-hexadecane, and the contact angles obtained for individual smooth colloidal probes. The single-particle contact angle θ_f was extracted from the maximal capillary force F_{max} by means of eq 2.[36,38] θ_s denotes the static contact angle, whereas θ_a and θ_r are the advancing and the receding droplet contact angles, respectively. The presence of contact angle hysteresis ($\theta_a \neq \theta_r$) suggests chemical inhomogeneity of the surface. The difference between θ_s and θ_r is particularly marked for the fluorinated surfaces. Also, as shown in Table 1, $\theta_f^{w/o}$ (for individual smooth colloids) and $\theta_r^{w/o}$ (for water droplets on model macroscopic surfaces) are in good agreement.

AFM Measurements. We now proceed to the results obtained for the detachment of the colloidal probes as a function of their surface chemistry and roughness. Before starting with each specific chemical modification, it is worth making an important premise. Previous experiments with rough fluorinated AFM probes carried out at both water/air and oil/air interfaces showed that at low applied loads, air pockets were trapped between the asperities.[48] As a consequence, the wetting was described by the CB regime. Conversely, in our case, all colloidal probe AFM experiments were carried out at water/*n*-hexadecane interfaces starting with a probe that is fully immersed in the oil. Moreover, as reported in Table 1, all $\theta_s^{o/a}$ values (for *n*-hexadecane droplets in air) are well below 90°, which suggest that all colloidal probes should be fully wetted by *n*-hexadecane before entering into the aqueous phase. The AFM experiments therefore start from a Wenzel state.

Colloidal Probes with OTS Functionalization. We will first describe the detachment of the OTS-modified particles as a function of their surface roughness, described by the parameter $\langle H\rangle/\langle d\rangle$. As mentioned in the introduction, the detachment force and distance are measured as a function of the load that is applied to the interface.

For comparable values of F_{load}, all retraction curves display the common features illustrated in Figure 1c. At a closer examination though, especially close to the maximal detachment force, several marked differences become evident (see Figure 3). The shape of the curve corresponding to the smooth probe has a rounded minimum around F_{max} (Figure 3, red line), and the value of D_{max} does not coincide with the one for D_0,[36] that is, the maximal force is reached before the maximal detachment distance D_0. For the rough probes, the detachment event is instead abrupt. The force−distance curve around F_{max} has a sharp "V-shape" (see Figure 3), and D_{max} and D_0 practically coincide (D_{max} and D_0 are also very close for small and hydrophobic particles, see the Supporting Information section 8). Moreover, for the smooth colloid (see the red curve), the force decreases smoothly and monotonically until

Table 1. Static ($\theta_s^{w/o}$), Advancing ($\theta_a^{w/o}$), and Receding ($\theta_r^{w/o}$) Contact Angles of Water Droplets on Chemically Modified Silicon Wafers Immersed in *n*-Hexadecane[a]

functionalization	$\theta_s^{w/o}$ (deg)	$\theta_a^{w/o}$ (deg)	$\theta_r^{w/o}$ (deg)	$\theta_f^{w/o}$ (deg)	$\theta_s^{o/a}$ (deg)	$\theta_a^{o/a}$ (deg)	$\theta_r^{o/a}$ (deg)
Br-silane	109 ± 1	116 ± 1	85 ± 4	89 ± 2	<10	<10	<10
OTS	151 ± 1	153 ± 2	147 ± 3	112 ± 2	59 ± 1	61 ± 1	46 ± 4
fluorosilane	140 ± 1	145 ± 1	112 ± 1	124 ± 1	80 ± 2	81 ± 1	73 ± 1

[a] $\theta_s^{o/a}$, $\theta_a^{o/a}$, and $\theta_r^{o/a}$ are the static, advancing, and receding contact angles measured for *n*-hexadecane droplets on the same wafers in air. $\theta_f^{w/o}$ is the contact angle calculated from the maximal adhesion force F_{max} for smooth colloidal probes detaching from a water/*n*-hexadecane interface and functionalized in the same way as the equivalent macroscopic surfaces.

DOI: 10.1021/acs.langmuir.8b00327
Langmuir XXXX, XXX, XXX−XXX

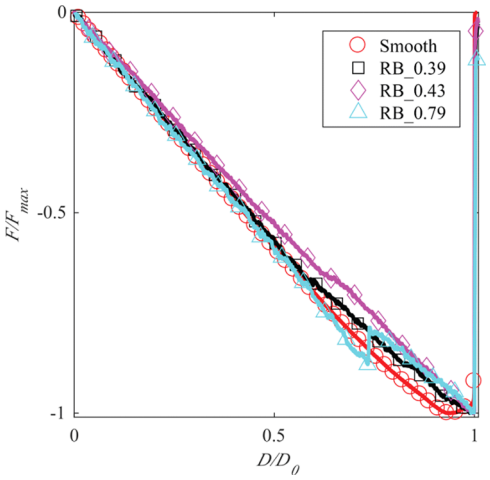

Figure 3. Retraction curves for OTS-modified colloidal probes. The red circles correspond to a smooth silica sphere, the black squares correspond to a rough colloid RB_0.39, the magenta diamonds are for a rough colloid RB_0.43, and the cyan triangles are for a rough colloid RB_0.79. The curves are normalized by the respective maximum detachment forces F_{max} and the maximum detachment distances D_0.

F_{max}, whereas, for the rougher colloids, the force−distance curves show visible oscillations and even sawtooth jumps (see the black and cyan curves in Figure 3). These qualitative differences clearly show that the detachment mechanisms for the different colloids depend significantly on the surface roughness.

Starting from these qualitative traits, a more detailed quantitative comparison between the different surfaces can be made. As described in the Introduction, we can vary the applied load F_{load}, with which the colloid is pushed toward the interface (Figure 1d) and measure the corresponding detachment force F_{max}. In Figure 4a, we plot the maximal capillary force F_{max} as a function of the load F_{load} for all roughness classes. For the smooth colloids, where F_{max} depends only on the particle contact angle θ (see eq 2), F_{max} is not expected to depend on F_{load}. This is confirmed by the red data points in Figure 4a. A constant F_{max} means that the contact line can slide smoothly on the colloid's surface during the retraction process, thus fulfilling the boundary condition for a constant contact angle. This result directly confirms that the OTS-modified colloids and wafers have uniform surface chemistry, justified also by the small contact angle hysteresis observed in the macroscopic measurements (Table 1). The contact-line sliding regime is also quantitatively confirmed by the mismatch between D_0 and D_{max}, as reported in Figure 4b (red histogram) and as previously investigated for a broad range of smooth colloids.[36] Furthermore, the distribution of the maximal detachment force F_{max} is rather narrow (see Figure 4c—the red histogram).

Interestingly, the OTS-modified rough particles also show a very weak dependence of F_{max} as a function of F_{load} for all roughness classes. Nevertheless, this result has a completely different origin. In fact, in the case of rough particles, the detachment mechanism is characterized by the contact-line pinning regime. In the presence of pinning, as mentioned above, the detachment event is abrupt, and the force−distance curve around F_{max} has a sharp "V-shape" (see Figure 3), which translates into the coincidence of D_{max} with D_0. This is confirmed in Figure 4b (the blue histogram). A constant value of F_{max} versus F_{load} would then indicate that the contact line was pinned at the same position on the probe surface for all detachment curves. The presence of multiple values of F_{max} for the same value of the loading force F_{load} shows that the detachment process is more complicated and that there may be a multitude of effective pinning sites on the probe surface (Figure 4c; RB_0.39). Finally, we observe that the values of the detachment forces for the rough colloids are significantly lower than the values of the detachment forces for the smooth colloids (Figure 4a), implying that the rough colloids possess a higher receding contact angle than the smooth colloids, as it will be discussed later.

AFM Colloidal Probes with Fluoro Functionalization. We then move to the case of fluoro-functionalized colloidal probes. Similar to the OTS-modification, F_{max} does not depend on F_{load} for the smooth particles (Figure 5a). Nevertheless, a distinct difference is seen when we examine the distribution of the D_0/D_{max} values, as shown in Figure 5b. We can identify two

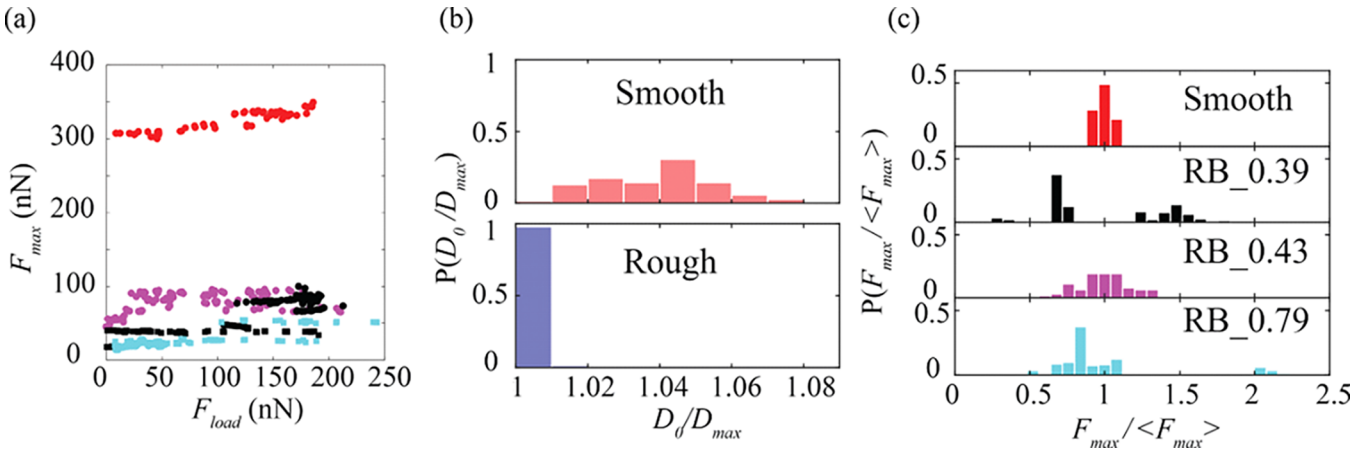

Figure 4. (a) Maximal detachment force F_{max} vs load F_{load} applied on the interface during the approach of the OTS-modified probes. Attachment−detachment repetitions of the same colloid are plotted with the same color and symbol. Different symbols of the same color represent different experiments carried out with different colloidal probes having the same surface morphology and the same functionalization. Red: smooth particles $\langle H\rangle/\langle d\rangle \approx 0$; black: RB_0.39; magenta: RB_0.43; cyan: RB_0.79. (b) Probability distributions of the D_0/D_{max} ratios for smooth (top) and rough colloids (bottom—all roughness classes are grouped together). The D_0/D_{max} values that are closest to 1 are a signature of pinning. (c) Probability distributions of the normalized detachment force $F_{max}/\langle F_{max}\rangle$ for the various roughness classes [same colors as in (a)].

DOI: 10.1021/acs.langmuir.8b00327
Langmuir XXXX, XXX, XXX−XXX

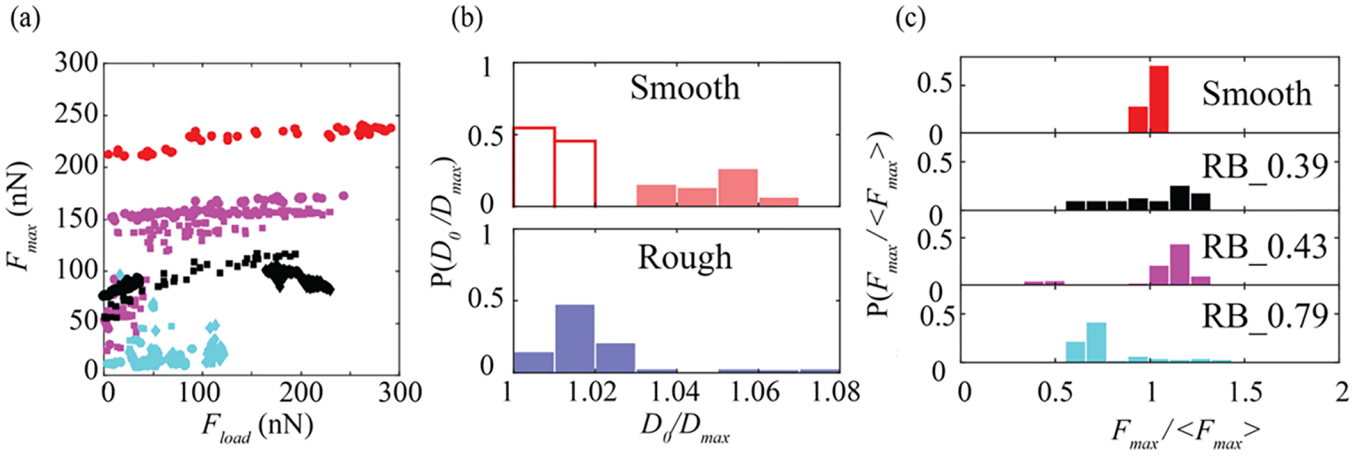

Figure 5. (a) Maximal detachment force F_{max} vs load F_{load} applied on the interface during the approach of fluorinated probes. Attachment−detachment repetitions of the same colloid are plotted with the same color and symbol. Different symbols of the same color represent different experiments carried out with different colloidal probes having the same surface morphology and the same functionalization. Red: smooth particles $\langle H\rangle/\langle d\rangle \approx 0$; black: RB_0.39; magenta: RB_0.43; cyan: RB_0.79. (b) Probability distributions of the D_0/D_{max} ratios for smooth (top) and rough colloids (bottom—all roughness classes are grouped together). The D_0/D_{max} values that are closest to 1 are a signature of pinning. For the topographically smooth but chemically heterogeneous probes, detachment events have been divided: for pinning (empty histogram bars) and for sliding (filled histogram bars). (c) Probability distributions of the normalized detachment force $F_{max}/\langle F_{max}\rangle$ for the various roughness classes [same colors as in (a)].

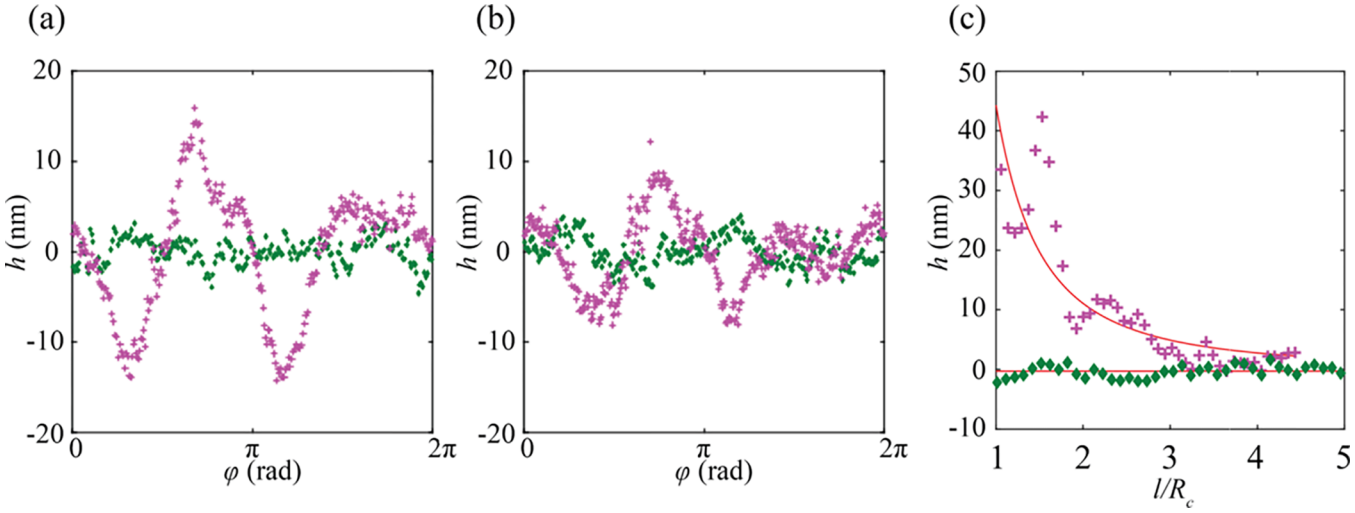

Figure 6. Interfacial deformations around isolated hydrophobized smooth silica particles measured using AFM on a replica of the interface. The interface height profiles are plotted vs the angular position along the contact line at a distance of 300 nm (a) and 500 nm (b) from the particle edge, respectively. Magenta crosses: PPFS-modified particles; green diamonds: OTS-modified particles. (c) The interface height is depicted as a function of the radial distance l (at a fixed angle φ along the perimeter). The red lines are fits according to eq 3.

different populations of detachment events (more details in the Supporting Information section 4): one with D_0/D_{max} values closer to 1 (empty red histogram) and another one with larger values (filled red histogram). Given the discussion above, the two populations correspond to contact-line pinning and sliding, respectively. This behavior stems from the presence of chemical heterogeneities on the particle surfaces, which are also present in the smooth wafer with fluoro functionalization, as reflected by the large contact angle hysteresis reported in Table 1 (see the Supporting Information section 5 for more details). The chemical heterogeneities appear to be sufficient to induce some local pinning during the repeated wetting/dewetting cycles. In spite of this fact, a very narrow distribution of F_{max} is observed for the smooth fluoro-modified particles (Figure 5c, red histogram), suggesting that the wettability of the various chemical patches does not differ significantly, so as to produce large variations in the adhesion forces.

For the fluoro-functionalized rough colloids, we find a behavior that is qualitatively similar to that of the OTS-modified particles. However, by applying a chemically heterogeneous fluorinated layer on the geometrically rough surface, we observe an even higher degree of hydrophobicity[6,11,45] and a broader distribution of pinning points. As a result, oscillations and jumps in the force close to F_{max} occur (see Supporting Information section 4), and the distribution of D_0/D_{max} becomes significantly broader.

The pinning detachment observed for the fluorinated smooth particles was the object of additional investigations to confirm the presence of chemical heterogeneities further. As predicted by theory[56,59,60] and recently proven experimentally,[15] contact-line pinning around rough spherical particles leads to

DOI: 10.1021/acs.langmuir.8b00327
Langmuir XXXX, XXX, XXX−XXX

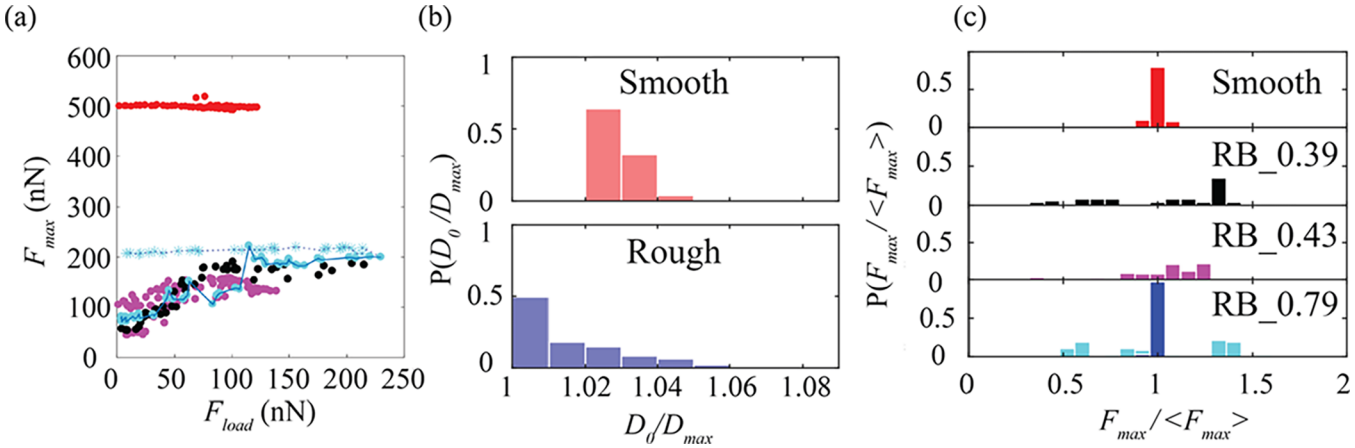

Figure 7. (a) Maximal detachment force F_{max} vs load F_{load} applied on the interface during the approach of Br-silane-modified probes. Attachment−detachment repetitions of the same colloid are plotted with the same color and symbol. Different symbols of the same color represent different experiments carried out with different colloidal probes having the same surface morphology and the same functionalization. Red: smooth particles $\langle H\rangle/\langle d\rangle \approx 0$; black: RB_0.39; magenta: RB_0.43; cyan: RB_0.79. The cyan curve is split into two segments; the dots represent the ramp-up of F_{load}, and the asterisks depict the ramp-down of F_{load}. (b) Probability distributions of the D_0/D_{max} ratios for smooth (top) and rough colloids (bottom—all roughness classes are grouped together). The D_0/D_{max} values that are closest to 1 are a signature of pinning. (c) Probability distributions of the normalized detachment force $F_{max}/\langle F_{max}\rangle$ for the various roughness classes [same colors as in (a)] with the exception of the bottom panel, where in cyan are depicted the data for the rough particles RB_0.79 during the ramp-up of F_{load}, whereas in blue during the ramp-down of F_{load}.

corrugated interfaces with a quadrupolar interfacial deformation in the far field. Similar interfacial deformations are also expected for chemically heterogeneous colloids trapped at liquid interfaces,[56,59−61] but have not yet been directly confirmed at the single-particle level. We tested this hypothesis by using PPFS-modified silica colloids (see the Experimental Section for details), which retain a topographically smooth surface after chemical modification, as shown in the Supporting Information section 5. By comparing the heights of the interface at various distances from the particle contact line (Figure 6a,b), we see that the OTS-modified colloids impart negligible interface deformations, whereas the PPFS-modified colloids induce larger corrugations of the interface. The symmetry of the deformation is quadrupolar. In fact, the vicinity of the particle, sitting at the interface, represents a saddle, possessing two peaks and two valleys. The height of the peaks (or the depth of the valleys) decays as $(1/l)^2$, as predicted by the capillary theory[56] (Figure 6c). These additional observations confirm that the fluorinated silica particles are geometrically smooth but chemically heterogeneous; hence, they induce contact-line pinning upon detachment. Further experiments carried out on macroscopic flat wafers, corroborating this hypothesis, can be found in the Supporting Information sections 5 and 6.

AFM Colloidal Probes with Bromo Functionalization. In a third set of experiments, we applied a surface modification using a Br-silane layer, giving contact angles close to neutral wetting.[15] Correspondingly, Br-silane-modified smooth particles give higher values of the detachment force compared to the values of F_{max} measured for the OTS and fluoro modifications. For such smooth particles, the retraction curves are fully compatible with contact-line sliding, and the distribution of F_{max} is very narrow (Figure 7). Compared to the more hydrophobic coatings, the Br-silane-modified rough colloidal probes present a distinctively more complex detachment behavior. First, all three roughness categories exhibit an almost linear increase of the adhesion force F_{max} with F_{load} up to $F_{load} \approx 100$ nN. For loads higher than this threshold value, F_{max} practically levels off as a function of F_{load} (especially visible for RB_0.39 and RB_0.79). The observed trends are reversible for roughness classes RB_0.39 and RB_0.43. The particles RB_0.79 present a markedly different behavior instead, namely the F_{max} versus F_{load} plot shows hysteresis upon increasing and decreasing loads. The hysteresis indicates that the colloidal probe changed its wetting properties during the experiments. A plausible explanation for the changed wetting properties may come from water impalement in between the surface asperities. Indeed, the very large surface roughness of the RB_0.79 particles can give rise to external layers with open porosity, in which water may fully and irreversibly penetrate, thus permanently displacing the *n*-hexadecane (water impalement). For the sake of simplicity, we assume that the depinning (impalement) pressure for a square lattice corresponds to the minimal threshold pressure needed for permanent water entrapment.[11,48] The impalement pressure for a square lattice constitutes a lower limit compared to other geometries, for example, asperities forming a hexagonal lattice. The driving force for liquid impalement is the capillary pressure P_c, associated with the liquid cavity formed by the microparticle. Then, $P_c \approx \frac{2\gamma}{R} = 34$ kPa, where $R \approx 3.1$ μm is the microparticle radius and $\gamma = 53$ mN/m. By assuming that the berry-to-berry distance $\langle d\rangle$ coincides with the lattice constant, the depinning pressure is $P^s_{dep} = \frac{2\pi\gamma r}{\langle d\rangle^2}\sin^2\left(\frac{\theta_a}{2}\right)$, where r is the radius of the berry. By replacing θ_a with the values reported in Table 1, the minimal impalement pressures are 71 kPa for the bromo functionalization, 94 kPa for the OTS-modified particles, and 90 kPa for the fluorosilane-modified particles RB_0.79. All values are higher than the capillary pressure, so water imbibition should be prevented, but the lower value for the bromo functionalization indicates that those particles would be the first to show impalement. Discrepancies with the estimates above may come from the presence of large values of d for some asperities, which are underestimated by only considering $\langle d\rangle$ and for which P_c may approach P^s_{dep}. Finally, as discussed in the Supporting Information section 3, for particles with more hydrophilic surfaces, water imbibition may even become

DOI: 10.1021/acs.langmuir.8b00327
Langmuir XXXX, XXX, XXX−XXX

spontaneous. This event does not occur for other roughness classes, for which no open porosity exists.

For all bromosilane-modified rough particles, D_0/D_{max} is very close to 1, indicative of strong contact-line pinning. The trend of $F_{max}/\langle F_{max}\rangle$, already observed for the other two surface modifications, is further confirmed for the less hydrophobic bromosilane: with increasing $\langle H\rangle/\langle d\rangle$-values, the distribution of the maximal adhesion force F_{max} becomes broader. Interestingly, the water-imbibed colloidal probe presents a very narrow distribution of F_{max}. This result together with the data for D_0/D_{max} reported in Figure 7b confirm that the liquid imbibition creates a complex surface consisting of islands of chemically modified silica that are surrounded by a layer of water entrapped in the porous structure. Such a representation is in agreement with the results obtained by Paunov et al.[62,63] for infused porous macroparticles at liquid interfaces, where the induced surface heterogeneity behaves as a conventional inhomogeneous surface and is able to pin the contact line upon detachment.

Comparison between the Different Surface Functionalizations. Finally, we will compare the behavior observed for the different chemical functionalizations. With the exception of the fluorinated particles, the smooth probes behave as expected. All detachment events proceed via contact-line sliding, and the values of the maximal force F_{max} are narrowly distributed. In line with the macroscopic contact angle measurements, we observed an increase in the single-particle contact angle $\theta_f^{w/o}$ when more hydrophobic functionalizations are used, as reported in Table 1.

The detachment is more complex for the rough colloids because, as observed in the F_{max} versus F_{load} plots, F_{max} is not single-valued. Instead, F_{max} versus F_{load} either presents distinct terraces (OTS and fluoro modifications) or an increasing F_{max} with increasing F_{load}, followed by a plateau (Br-silane modification). In particular, the presence of multiple plateaus suggests a sudden change in the contact line position. In this regard, we calculated the number of asperities encompassed by the contact line corresponding to a given plateau value of F_{max}. From the plateau values of F_{max}, we can calculate the apparent contact angle of the colloidal probe $\theta_{r,app}$ (using eq 2) and thus determine the radius of the spherical cap exposed to water, equal to $R \sin \alpha_{max}$. The perimeter of the contact line projection on the core particle ($=2\pi R \sin \alpha_{max}$) can be divided by the average asperity-to-asperity distance $\langle d\rangle$ (Figure 2c) to obtain the number of asperities wetted by the contact line N_L. The equation for N_L reads

$$N_L = \frac{2\pi R \sin \alpha_{max}}{\langle d\rangle} = \frac{2\pi R \cos(\theta_{r,app}/2)}{\langle d\rangle} = \frac{1}{\langle d\rangle}\sqrt{\frac{2\pi R F_{max}}{\gamma}} \quad (4)$$

Table 2 summarizes the number of asperities extracted from the location of the contact line at the moment of detachment (N_L).

N_L decreases with the increase of $\langle d\rangle$ (see Figure 2c and Table S1), suggesting that the pinning of the contact line at the asperities correctly describes the detachment process. This result has important implications for the description of heterogeneous particles at liquid interfaces. In fact, it introduces an additional engineering tool for tuning the contact angle of colloids similar to the case of macroscopic surfaces.[3,4,11]

Table 2. Number of Asperities Extracted from the Location of the Contact Line at the Moment of Detachment (N_L) for Three Different Functionalizations

	Br-silane	OTS	fluorosilane
$\langle H\rangle/\langle d\rangle$ class	N_L	N_L	N_L
RB_0.39	16.3	5.2	11.6
		7.3	
		10.3	
RB_0.43	40.5	32.4	40.3
RB_0.79	6.6	2.6	1.8
		3.3	

The number and size of the asperities involved during detachment affect not only F_{max} and D_0 but also the motion of the contact line in general. The latter either moves (slides) over the smooth surfaces or experiences a more discontinuous motion over the rough surfaces, as qualitatively shown in Figure 3. The continuity of the contact-line motion can be captured by quantifying the oscillations of the retraction curves for the different functionalizations and particle roughness classes, as reported in Figure 8a. We notice that the root-mean-square error (RMSE) of the curves relative to their respective baselines (obtained via the second smoothing procedure described in the Experimental Section) increases by increasing the particle roughness. The detachment of rough particles proceeds through multiple subevents of contact-line stick-slip, leading to jumps in the force−distance curve, which contribute to the RMSE of the oscillations.

Finally, we observe in Figure 8b that $\langle F_{max}\rangle$ steadily decreases when the roughness increases. Consequently, as shown in Figure 8c, the contact angle increases to the point where very hydrophobic particles are obtained in the case of rough colloids hydrophobized by OTS and fluorosilanes.

Interestingly, the wetting behavior reported here presents some crucial differences compared to the dewetting of larger superamphiphobic probes at water/air interfaces.[48] In the work by Ye et al.,[48] two regimes of dewetting were found as a function of the applied load. At low loads, F_{max} steeply increased with F_{load}, indicating that an increasing (yet small) number of asperities was wetted upon increasing indentation. At higher loads, F_{max} showed instead a gradual linear dependence on F_{load}, stemming from the force required to depin the contact line that had moved over a large and load-dependent number of asperities.

CONCLUSIONS

In this work, we focused on the desorption of rough particles from water/oil interfaces using colloidal probe AFM. Although a very limited number of particles can be measured using this technique, a wealth of information is extracted. In particular, we investigated the role of surface roughness and surface chemistry on the nature of the detachment. In general, we observed that for hydrophobic particles, increasing the surface roughness changes the type of detachment mechanism from contact-line sliding to contact-line pinning. This fact is qualitatively underlined by a change in the shape of the force−distance curve close to the detachment point and quantitatively confirmed by the different distributions of D_0/D_{max} for the two detachment regimes, that is, detachment upon contact-line sliding or contact-line pinning. As previously observed,[15] rough colloidal probes approaching the interface from the apolar phase are rendered effectively more hydrophobic. Additionally,

DOI: 10.1021/acs.langmuir.8b00327
Langmuir XXXX, XXX, XXX−XXX

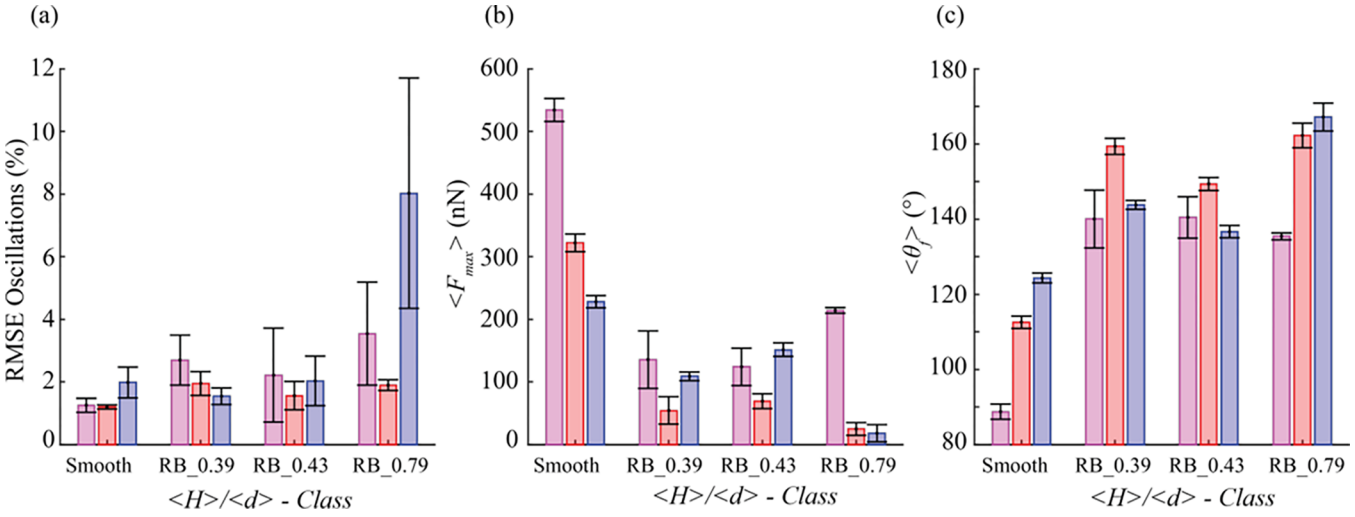

Figure 8. Comparison between the different surface functionalizations as a function of the roughness. (a) RMSE of the oscillations of the retraction curve. (b,c) are the average maximal detachment force and the apparent particle contact angle, respectively. (c) was calculated from (b) by means of eq 2. Colors: magenta, bromo-functionalization; red, OTS; blue, fluorosilane.

roughening the surfaces of the probes introduces a multitude of pinning and detachment points and leads to a broader relative distribution of the detachment forces and distances. The former correlates with the number of asperities wetted by the contact line before detaching. The increased noise observed in the force signal of heterogeneous probes during the retraction further confirms that the contact line does not undergo a single-step detachment. Conversely, the detachment process can be split into discrete rearrangements of the contact line until the particle is removed from the interface.

All these considerations have direct implications for the use of nonideal particles at liquid interfaces, and in particular, for the destabilization of Pickering emulsions and foams. In fact, the detachment energy of a colloidal particle depends on the cross-sectional area it can share with the interface. Rough particles, which do adsorb in metastable positions, allow for the tuning of the protrusion height and thus the exposed cross-sectional area. As a consequence, the detachment distance becomes a function of the energy used to bring the particles to the interface. Therefore, higher energy inputs during an emulsification process may bring a higher number of asperities in contact with the interface, thus leading to an enhancement of the particle detachment force and hence to the improved stability of the resulting emulsion. For recovery purposes, where the stabilizing particles must be collected afterward, for example, in oil separation and particle recovery, low detachment forces, which could be achieved by roughness tailoring, are instead favored. Additional options are also offered when rough surfaces can be imbibed by a fluid different from the one in which they are initially dispersed. This may allow the CB regime to be suppressed[48] or modified, switching from an oil-soaked to a water-impaled state. These two different cases may lead to a complete switch of the particle wettability depending on the contact angle of the single asperities.[62,63] In conclusion, these findings emphasize the interesting role played by surface heterogeneities in interfacial phenomena, highlighting the potential of tailoring the surface roughness and chemistry in the design of new particle-based materials.

■ ASSOCIATED CONTENT

Supporting Information

The Supporting Information is available free of charge on the ACS Publications website at DOI: 10.1021/acs.langmuir.8b00327.

Additional experimental details about the fabrication and characterization of the particles and surfaces used in this work, in particular, the reaction parameters for the fabrication of the all-silica raspberry-like particles; a detailed study of the asperity shape; measurements of rms roughness; a quantitative discussion on the *n*-hexadecane and water impalement for different particle surfaces; a detailed insight on the observed detachment mechanisms; a close inspection of the surface heterogeneity observed for flat and spherical fluorinated silica surfaces; a complementary analysis of the detachment of a fluorinated colloidal probe presenting a FIB-sculpted notch; and a comparative analysis of the differences between the maximum detachment distance and the distance at maximum force for contact-line sliding (PDF)

■ AUTHOR INFORMATION

Corresponding Author

*E-mail: lucio.isa@mat.ethz.ch.

ORCID

Alla Synytska: 0000-0002-0643-7524
Svetoslav E. Anachkov: 0000-0002-2417-1539
Lucio Isa: 0000-0001-6731-9620

Author Contributions

M.Z., I.L., S.E.A., and L.I. planned and designed the research. I.L. and M.Z. performed the AFM measurements. M.Z., E.M., and C.-P.H. fabricated the colloidal probes. C.M. and A.S. provided the reference heterogeneous fluoro-modified particles. S.E.A. wrote the roughness measurement codes for AFM image analysis. M.Z. and L.I. wrote the manuscript. All authors analyzed and discussed the data and proofread the manuscript.

Notes

The authors declare no competing financial interest.

DOI: 10.1021/acs.langmuir.8b00327
Langmuir XXXX, XXX, XXX−XXX

■ ACKNOWLEDGMENTS

L.I. and M.Z. acknowledge the financial support from the Swiss National Science Foundation (grant PP00P2_144646/1). L.I., I.L., and S.E.A. acknowledge the financial support from the Scientific Exchange Programme NMS.CH grants Sciex 14.081 and Sciex 14.082. S.E.A. and I.L. acknowledge the financial support from the Horizon 2020 project ID: 692146-H2020-eu.4.b "Materials Networking."

■ REFERENCES

(1) Young, T. An Essay on the Cohesion of Fluids. *Phil. Trans. Roy. Soc. Lond.* **1805**, *95*, 65−87.
(2) de Gennes, P. G. Wetting: statics and dynamics. *Rev. Mod. Phys.* **1985**, *57*, 827−863.
(3) Wenzel, R. N. Resistance of solid surfaces to wetting by water. *Ind. Eng. Chem.* **1936**, *28*, 988−994.
(4) Cassie, A. B. D.; Baxter, S. Wettability of porous surfaces. *Trans. Faraday Soc.* **1944**, *40*, 546−551.
(5) Barthlott, W.; Neinhuis, C. Purity of the sacred lotus, or escape from contamination in biological surfaces. *Planta* **1997**, *202*, 1−8.
(6) Ming, W.; Wu, D.; van Benthem, R.; de With, G. Superhydrophobic Films from Raspberry-like Particles. *Nano Lett.* **2005**, *5*, 2298−2301.
(7) Tsai, H.-J.; Lee, Y.-L. Facile Method to Fabricate Raspberry-like Particulate Films for Superhydrophobic Surfaces. *Langmuir* **2007**, *23*, 12687−12692.
(8) Wong, T.-S.; Kang, S. H.; Tang, S. K. Y.; Smythe, E. J.; Hatton, B. D.; Grinthal, A.; Aizenberg, J. Bioinspired self-repairing slippery surfaces with pressure-stable omniphobicity. *Nature* **2011**, *477*, 443−447.
(9) Tuteja, A.; Choi, W.; Ma, M.; Mabry, J. M.; Mazzella, S. A.; Rutledge, G. C.; McKinley, G. H.; Cohen, R. E. Designing Superoleophobic Surfaces. *Science* **2007**, *318*, 1618−1622.
(10) Deng, X.; Mammen, L.; Butt, H.-J.; Vollmer, D. Candle Soot as a Template for a Transparent Robust Superamphiphobic Coating. *Science* **2012**, *335*, 67−70.
(11) Butt, H.-J.; Semprebon, C.; Papadopoulos, P.; Vollmer, D.; Brinkmann, M.; Ciccotti, M. Design principles for superamphiphobic surfaces. *Soft Matter* **2013**, *9*, 418−428.
(12) Amabili, M.; Giacomello, A.; Meloni, S.; Casciola, C. M. Collapse of superhydrophobicity on nanopillared surfaces. *Phys. Rev. Fluids* **2017**, *2*, 034202.
(13) Pieranski, P. Two-Dimensional Interfacial Colloidal Crystals. *Phys. Rev. Lett.* **1980**, *45*, 569−572.
(14) Stocco, A.; Nobili, M. A comparison between liquid drops and solid particles in partial wetting. *Adv. Colloid Interface Sci.* **2017**, *247*, 223−233.
(15) Zanini, M.; Marschelke, C.; Anachkov, S. E.; Marini, E.; Synytska, A.; Isa, L. Universal emulsion stabilization from the arrested adsorption of rough particles at liquid-liquid interfaces. *Nat. Commun.* **2017**, *8*, 15701.
(16) San-Miguel, A.; Behrens, S. H. Influence of Nanoscale Particle Roughness on the Stability of Pickering Emulsions. *Langmuir* **2012**, *28*, 12038−12043.
(17) Mable, C. J.; Warren, N. J.; Thompson, K. L.; Mykhaylyk, O. O.; Armes, S. P. Framboidal ABC triblock copolymer vesicles: a new class of efficient Pickering emulsifier. *Chem. Sci.* **2015**, *6*, 6179−6188.
(18) Binks, B. P.; Rodrigues, J. A. Types of Phase Inversion of Silica Particle Stabilized Emulsions Containing Triglyceride Oil. *Langmuir* **2003**, *19*, 4905−4912.
(19) Kaz, D. M.; McGorty, R.; Mani, M.; Brenner, M. P.; Manoharan, V. N. Physical ageing of the contact line on colloidal particles at liquid interfaces. *Nat. Mater.* **2012**, *11*, 138−142.
(20) Wang, A.; McGorty, R.; Kaz, D. M.; Manoharan, V. N. Contact-line pinning controls how quickly colloidal particles equilibrate with liquid interfaces. *Soft Matter* **2016**, *12*, 8958−8967.
(21) Boniello, G.; Blanc, C.; Fedorenko, D.; Medfai, M.; Mbarek, N. B.; In, M.; Gross, M.; Stocco, A.; Nobili, M. Brownian diffusion of a partially wetted colloid. *Nat. Mater.* **2015**, *14*, 908−911.
(22) Binks, B. P.; Clint, J. H.; Mackenzie, G.; Simcock, C.; Whitby, C. P. Naturally Occurring Spore Particles at Planar Fluid Interfaces and in Emulsions. *Langmuir* **2005**, *21*, 8161−8167.
(23) Nonomura, Y.; Kobayashi, N.; Nakagawa, N. Multiple Pickering Emulsions Stabilized by Microbowls. *Langmuir* **2011**, *27*, 4557−4562.
(24) Pitois, O.; Chateau, X. Small Particle at a Fluid Interface: Effect of Contact Angle Hysteresis on Force and Work of Detachment. *Langmuir* **2002**, *18*, 9751−9756.
(25) Poulichet, V.; Garbin, V. Ultrafast desorption of colloidal particles from fluid interfaces. *Proc. Natl. Acad. Sci. U.S.A.* **2015**, *112*, 5932−5937.
(26) Menon, V. B.; Nagarajan, R.; Wasan, D. T. Separation of Fine Particles from Nonaqueous Media: Free Energy Analysis and Oil Loss Estimation. *Sep. Sci. Technol.* **1987**, *22*, 2295−2322.
(27) Preuss, M.; Butt, H.-J. Direct measurement of forces between particles and bubbles. *Int. J. Miner. Process.* **1999**, *56*, 99−115.
(28) Preuss, M.; Butt, H.-J. Measuring the Contact Angle of Individual Colloidal Particles. *J. Colloid Interface Sci.* **1998**, *208*, 468−477.
(29) Preuss, M.; Butt, H.-J. Direct Measurement of Particle−Bubble Interactions in Aqueous Electrolyte: Dependence on Surfactant. *Langmuir* **1998**, *14*, 3164−3174.
(30) Butt, H.-J. A Technique for Measuring the Force between a Colloidal Particle in Water and a Bubble. *J. Colloid Interface Sci.* **1994**, *166*, 109−117.
(31) Ducker, W. A.; Xu, Z.; Israelachvili, J. N. Measurements of Hydrophobic and DLVO Forces in Bubble-Surface Interactions in Aqueous Solutions. *Langmuir* **1994**, *10*, 3279−3289.
(32) Gillies, G.; Büscher, K.; Preuss, M.; Kappl, M.; Butt, H.-J.; Graf, K. Contact angles and wetting behaviour of single micron-sized particles. *J. Phys. Condens. Matter* **2005**, *17*, S445−S464.
(33) Yakubov, G. E.; Vinogradova, O. I.; Butt, H.-J. Contact angles on hydrophobic microparticles at water−air and water−hexadecane interfaces. *J. Adhes. Sci. Technol.* **2000**, *14*, 1783−1799.
(34) Mulvaney, P.; Perera, J. M.; Biggs, S.; Grieser, F.; Stevens, G. W. The Direct Measurement of the Forces of Interaction between a Colloid Particle and an Oil Droplet. *J. Colloid Interface Sci.* **1996**, *183*, 614−616.
(35) Snyder, B. A.; Aston, D. E.; Berg, J. C. Particle−Drop Interactions Examined with an Atomic Force Microscope. *Langmuir* **1997**, *13*, 590−593.
(36) Anachkov, S. E.; Lesov, I.; Zanini, M.; Kralchevsky, P. A.; Denkov, N. D.; Isa, L. Particle detachment from fluid interfaces: theory vs. experiments. *Soft Matter* **2016**, *12*, 7632−7643.
(37) Gibbs, J. W. *The Collected Works of J. Willard Gibbs*; Yale University Press: New Haven, CT, 1957; Vol. *1*.
(38) Scheludko, A. D.; Nikolov, D. Measurement of surface tension by pulling a sphere from a liquid. *Colloid Polym. Sci.* **1975**, *253*, 396−403.
(39) Scheludko, A.; Toshev, B. V.; Bojadjiev, D. T. Attachment of particles to a liquid surface (capillary theory of flotation). *J. Chem. Soc. Faraday Trans. I* **1976**, *72*, 2815−2828.
(40) Ally, J.; Kappl, M.; Butt, H.-J. Adhesion of Particles with Sharp Edges to Air−Liquid Interfaces. *Langmuir* **2012**, *28*, 11042−11047.
(41) Zanini, M.; Hsu, C.-P.; Magrini, T.; Marini, E.; Isa, L. Fabrication of rough colloids by heteroaggregation. *Colloids Surf., A* **2017**, *532*, 116−124.
(42) Kamp, M.; Hermes, M.; van Kats, C. M.; Kraft, D. J.; Kegel, W. K.; Dijkstra, M.; van Blaaderen, A. Selective Depletion Interactions in Mixtures of Rough and Smooth Silica Spheres. *Langmuir* **2016**, *32*, 1233−1240.
(43) Furusawa, K.; Anzai, C. Preparation of composite fine particles by heterocoagulation. *Colloid Polym. Sci.* **1987**, *265*, 882−888.
(44) Harley, S.; Thompson, D. W.; Vincent, B. The adsorption of small particles onto larger particles of opposite charge Direct electron microscope studies. *Colloids Surf.* **1992**, *62*, 163−176.

DOI: 10.1021/acs.langmuir.8b00327
Langmuir XXXX, XXX, XXX−XXX

(45) D'Acunzi, M.; Mammen, L.; Singh, M.; Deng, X.; Roth, M.; Auernhammer, G. K.; Butt, H.-J.; Vollmer, D. Superhydrophobic surfaces by hybrid raspberry-like particles. *Faraday Discuss.* **2010**, *146*, 35−48.
(46) Graf, C.; Vossen, D. L. J.; Imhof, A.; van Blaaderen, A. A General Method To Coat Colloidal Particles with Silica. *Langmuir* **2003**, *19*, 6693−6700.
(47) Denkov, N.; Velev, O.; Kralchevski, P.; Ivanov, I.; Yoshimura, H.; Nagayama, K. Mechanism of formation of two-dimensional crystals from latex particles on substrates. *Langmuir* **1992**, *8*, 3183−3190.
(48) Ye, M.; Deng, X.; Ally, J.; Papadopoulos, P.; Schellenberger, F.; Vollmer, D.; Kappl, M.; Butt, H.-J. Superamphiphobic Particles: How Small Can We Go? *Phys. Rev. Lett.* **2014**, *112*, 016101.
(49) Kirillova, A.; Marschelke, C.; Friedrichs, J.; Werner, C.; Synytska, A. Hybrid Hairy Janus Particles as Building Blocks for Antibiofouling Surfaces. *ACS Appl. Mater. Interfaces* **2016**, *8*, 32591−32603.
(50) Naik, V. V.; Städler, R.; Spencer, N. D. Effect of Leaving Group on the Structures of Alkylsilane SAMs. *Langmuir* **2014**, *30*, 14824−14831.
(51) Matyjaszewski, K.; Xia, J. Atom Transfer Radical Polymerization. *Chem. Rev.* **2001**, *101*, 2921−2990.
(52) Hutter, J. L.; Bechhoefer, J. Calibration of atomic-force microscope tips. *Rev. Sci. Instrum.* **1993**, *64*, 1868−1873.
(53) Paunov, V. N. Novel Method for Determining the Three-Phase Contact Angle of Colloid Particles Adsorbed at Air−Water and Oil−Water Interfaces. *Langmuir* **2003**, *19*, 7970−7976.
(54) Canny, J. A Computational Approach to Edge Detection. *IEEE Trans. Pattern Anal. Mach. Intell.* **1986**, *PAMI-8*, 679−698.
(55) Duda, R.; Hart, P. *Pattern Classification and Scene Analysis*; John Wiley and Sons, 1973.
(56) Stamou, D.; Duschl, C.; Johannsmann, D. Long-range attraction between colloidal spheres at the air-water interface: The consequence of an irregular meniscus. *Phys. Rev. E* **2000**, *62*, 5263−5272.
(57) Kralchevsky, P. A.; Denkov, N. D.; Danov, K. D. Particles with an Undulated Contact Line at a Fluid Interface: Interaction between Capillary Quadrupoles and Rheology of Particulate Monolayers. *Langmuir* **2001**, *17*, 7694−7705.
(58) Ruiz-Cabello, F. J. M.; Moazzami-Gudarzi, M.; Elzbieciak-Wodka, M.; Maroni, P.; Labbez, C.; Borkovec, M.; Trefalt, G. Long-ranged and soft interactions between charged colloidal particles induced by multivalent coions. *Soft Matter* **2015**, *11*, 1562−1571.
(59) Danov, K. D.; Kralchevsky, P. A. Capillary forces between particles at a liquid interface: General theoretical approach and interactions between capillary multipoles. *Adv. Colloid Interface Sci.* **2010**, *154*, 91−103.
(60) Danov, K. D.; Kralchevsky, P. A.; Naydenov, B. N.; Brenn, G. Interactions between particles with an undulated contact line at a fluid interface: Capillary multipoles of arbitrary order. *J. Colloid Interface Sci.* **2005**, *287*, 121−134.
(61) Chen, W.; Tan, S.; Huang, Z.; Ng, T.-K.; Ford, W. T.; Tong, P. Measured long-ranged attractive interaction between charged polystyrene latex spheres at a water-air interface. *Phys. Rev. E* **2006**, *74*, 021406.
(62) Paunov, V. N.; Al-Shehri, H.; Horozov, T. S. Attachment of composite porous supra-particles to air-water and oil-water interfaces: theory and experiment. *Phys. Chem. Chem. Phys.* **2016**, *18*, 26495−26508.
(63) Al-Shehri, H.; Horozov, T. S.; Paunov, V. N. Preparation and attachment of liquid-infused porous supra-particles to liquid interfaces. *Soft Matter* **2016**, *12*, 8375−8387.

DOI: 10.1021/acs.langmuir.8b00327
Langmuir XXXX, XXX, XXX−XXX

Supporting Information:
Detachment of rough colloids from liquid-liquid interfaces

Michele Zanini[1], Ivan Lesov[2], Emanuele Marini[1], Chiao-Peng Hsu[1], Claudia Marschelke[3], Alla Synytska[3], Svetoslav E. Anachkov[2] and Lucio Isa[1*]

[1]Laboratory for Interfaces, Soft Matter and Assembly, Department of Materials, ETH Zurich, Vladimir-Prelog Weg 5, 8093 Zürich, Switzerland.

[2]Department of Chemical and Pharmaceutical Engineering, Faculty of Chemistry and Pharmacy, Sofia University, 1 James Bourchier Avenue, 1164 Sofia, Bulgaria.

[3]Department of Polymer Interfaces, Leibniz Institute of Polymer Research, Hohe Strasse 6, D-01069 Dresden, Germany.

Key words: roughness; detachment; fluid interfaces; contact line pinning; colloidal probe atomic force microscopy

Corresponding author: lucio.isa@mat.ethz.ch

Table S1 Reaction parameters for the fabrication of all-silica raspberry-like particles used as rough colloidal probes. The reported quantities were used to modify 10 mg of particles. PD stands for polydisperse. RMS denotes the average root-mean-square roughness. <*H*> and <*d*> are the mean asperity height and the mean asperity-to-asperity distance measured after the smoothening step, respectively.

Roughness Class	**NP size (nm)**	**Injected TEOS (5 vol%) (mL)**	**RMS (nm)**	**<*H*> (nm)**	**<*d*> (nm)**	**<*H*>/<*d*>**
RB_0.39	250 PD	1.83	54.5 ± 5.1	205 ± 27	528 ± 197	0.39 ± 0.15
RB_0.43	72	0.39	17.5 ± 3.7	78 ± 15	187 ± 79	0.42 ± 0.19
RB_0.79	960&39	0.92	> 100	970 ± 36	1270 ± 278	0.76 ± 0.17

Supplementary section 1: Asperity shape

The qualitative impression that the roughness features consist of spherical caps is quantitatively proven by the 3D reconstruction of a single asperity. The experimental data in the region of interest are fitted with the analytical expression for a sphere. The root-mean-square error (RMSE) of the fit is 4.8 nm (the asperity radius determined from the fit is 128 nm), which proves that the asperities are indeed spherical caps with different heights.

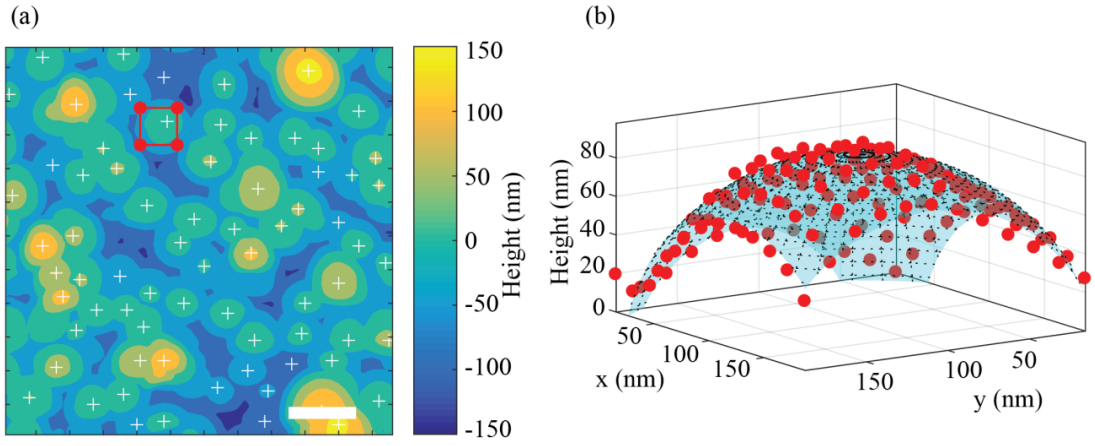

Figure S1 (a) Contour plot of the surface of a model rough particle (RB_0.39). The white crosses mark the asperities' centers of mass. The red square delimits the selected area that is used for the 3D reconstruction shown in panel (b). The scale bar is 300 nm. **(b)** 3D reconstruction of a single asperity. In red, we have shown the experimental points from the AFM scan. The cyan surface depicts the spherical fit. The fit root-mean-square error is 4.8 nm.

Supplementary section 2: RMS roughness

The particle surface topography can also be described by the root-mean-square (RMS) roughness. Using the RMS as a roughness descriptor, RB_0.39 and RB_0.43 are inverted, compared to the classification using the dimensionless parameter $\langle H \rangle / \langle d \rangle$ as in the manuscript.

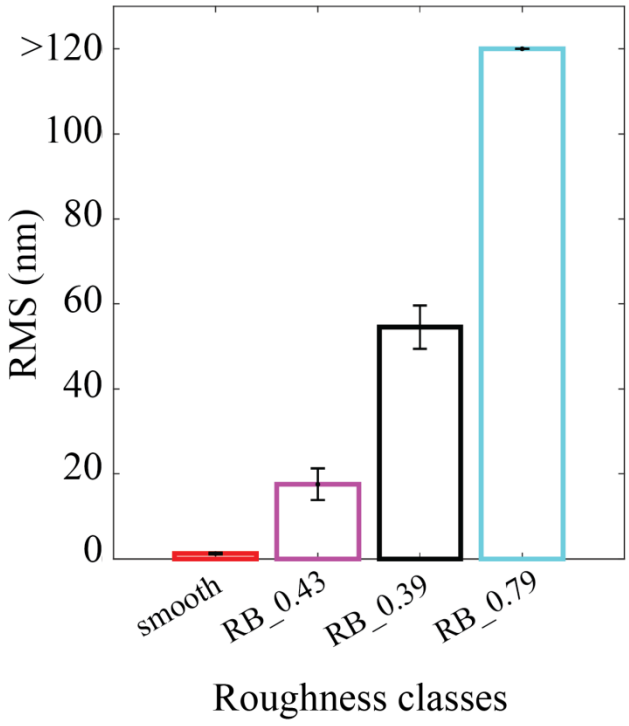

Figure S2 Model rough particles ranked in ascending order in terms of the RMS roughness. The same colors as in Figure 2 of the manuscript are used.

Supplementary section 3: n-hexadecane and water impalement

The n-hexadecane impalement is of particular interest for the rough particles RB_0.79. In fact, its enormous surface roughness could effectively act as open porosity. In this regard, the maximal driving force needed to fill the air pockets with n-hexadecane is given by the capillary pressure $P_c = \frac{2\gamma}{R} \approx 18$ kPa, where γ is the n-hexadecane surface tension in air (27.5 mN/m) and R = 3.1 µm is the particle radius. The capillary pressure for all the surface modifications is larger or comparable to the impalement pressure.

Table S2 Impalement pressure for n-hexadecane in air, calculated for the rough colloidal particles RB_0.79.

Functionalization	$P_{depinning}$ (kPa)
Br-silane	< 0.4
OTS	13.2
Fluoro-silane	21.7

For hydrophilic surface modifications, water impalement can take place spontaneously. This fact was proven with FreSCa [1-2] and GTT[3] measurements (see Figure S3a and b, respectively).

In Figure S3, the spontaneous water imbibition is clearly observed for particles RB_0.79 when the surface is hydrophilic. In fact, for the parameters reported in the manuscript, water impalement is expected for contact angles lower than $\theta = 2\arcsin\left(\frac{<d>}{\sqrt{\pi r R}}\right) \approx 72°$ ($<d>$ = 1270 nm, r = 480 nm, R = 3100 nm). Hence, surface topographies different than RB_0.79 cannot be impaled, even if they are hydrophilic, as reported in Figure S3c.

In both the FreSCa and GTT experiments, the rough particles were spontaneously adsorbed by sedimentation from the non-polar phase[4] (n-decane). FreSCa allows the visualization of the interface from the side previously occupied by the oil, while in GTT the interface is replicated and therefore imaged from the polar phase (water).

The amino functionalization was introduced by vigorously stirring the particles (few mg) in an aqueous mixture containing 0.6 vol% of APTES (3-(triethoxysilyl)propan-1-amine, >98%, Sial) for 24 h at room temperature. As reported in Table S3, the amino modification renders the surface hydrophilic.

Table S3 Macroscopic contact angles of water droplets on amino-modified silicon wafers immersed in n-hexadecane.

Functionalization	$\theta_s^{w/o}$(°)	$\theta_a^{w/o}$(°)	$\theta_r^{w/o}$(°)
APTES	63 ± 1	69 ± 2	29 ± 3

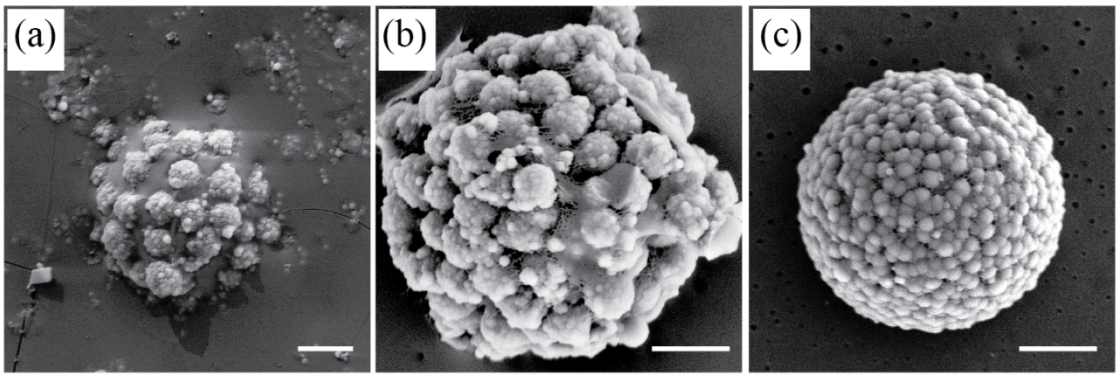

Figure S3 Hydrophilic particles imbibed by water during their spontaneous adsorption at the water/n-decane interface. **(a)** Unmodified RB_0.79 particle imaged with cryo-SEM. **(b)** GTT replica for a RB_0.79 particle modified with amino-silanes. **(c)** GTT replica for a RB_0.39 particle modified with amino-silane. In all cases, the scale bar is 2 μm.

Supplementary section 4: Pinning vs sliding detachment

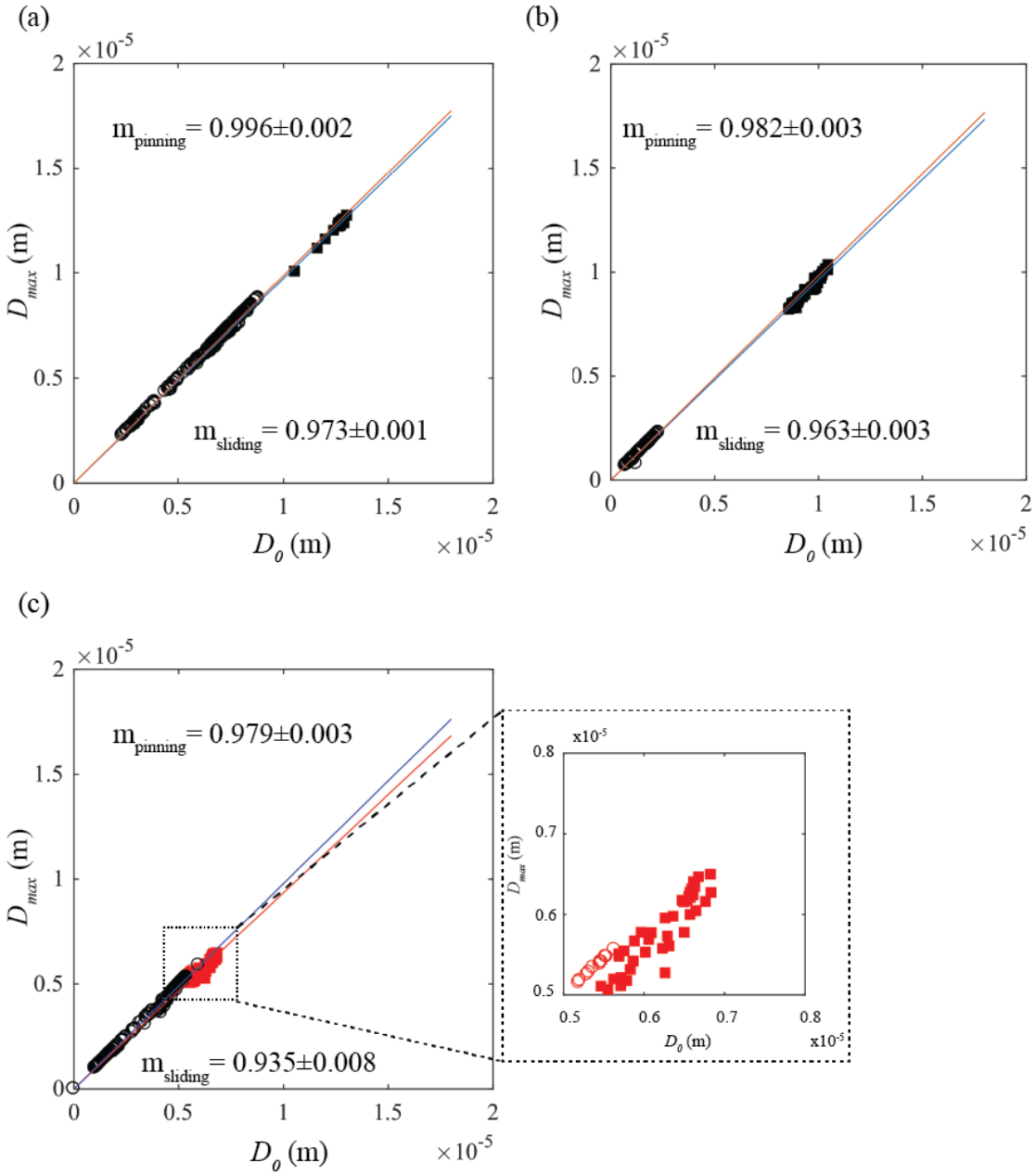

Figure S4 Linear fits of D_{max} versus D_0 for smooth and rough colloids with three different surface chemistries. **(a)** Bromo-functionalized, **(b)** OTS-modified and **(c)** fluoro-hydrophobized colloidal probes. Open circles represent the data for the rough colloids; black squares depict the data for the smooth particles. In panel **(c)**, the smooth particles presenting pinning-like behavior are plotted with red open circles, while smooth particles detaching via contact line sliding are reported with red squares. Blue lines depict the linear fits for the rough colloids and the red lines show the linear fits for the smooth particles, respectively. The *m*-values correspond to the slopes of the respective linear fits, showing statistically significant differences for pinning vs sliding detachment.

The qualitative difference between two force-distance curves of the same fluoro-hydrophobized rough colloid is shown in Figure S5. In both cases, pinning is expected and appears to have happened. Nevertheless, the strong oscillations of the red curve make the unequivocal determination of F_{max} challenging, as well as the determination of the actual

detachment position D_0. In the case of the red curve, the global minimum does not correspond to D_0. The latter gives rise to the upper tail in the distribution of D_0/D_{max}.

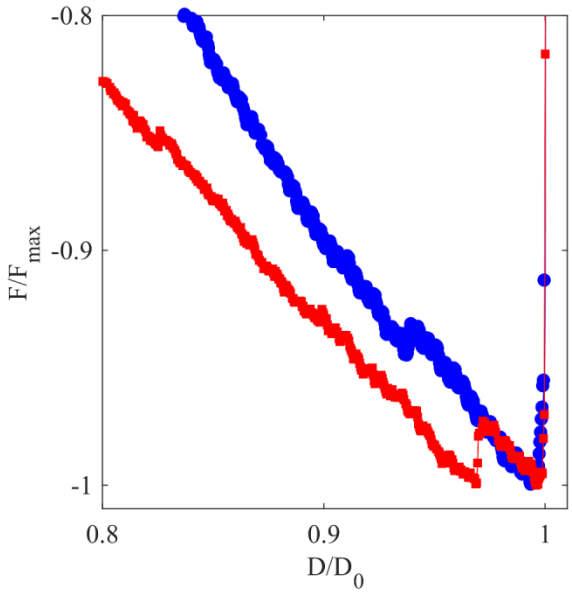

Figure S5 Retraction curves for a rough colloid (RB_0.39) modified with fluoro-silane. In blue, a curve that shows pinning detachment. In red, a (noisy) curve that shows sliding detachment.

Supplementary section 5: Investigation of fluorinated planar surfaces

A more detailed investigation of the surface of fluoro-silane-modified wafers revealed the appearance of sparse blobs when the wafer was scanned in water. In contrast, the same region of interest was found to be perfectly flat when scanned in air at ambient conditions (Figure S6). This morphological change has only a minor impact on the geometrical roughness of the surface, but it gives rise to a relevant chemical heterogeneity. Locally, non-uniform surface chemistries produce wetting discontinuities which can act as pinning points during the contact line motion[5]. The latter also explains the large contact angle hysteresis observed for the fluoro-silanized smooth particles, which directly affects the force-distance curves for such particles.

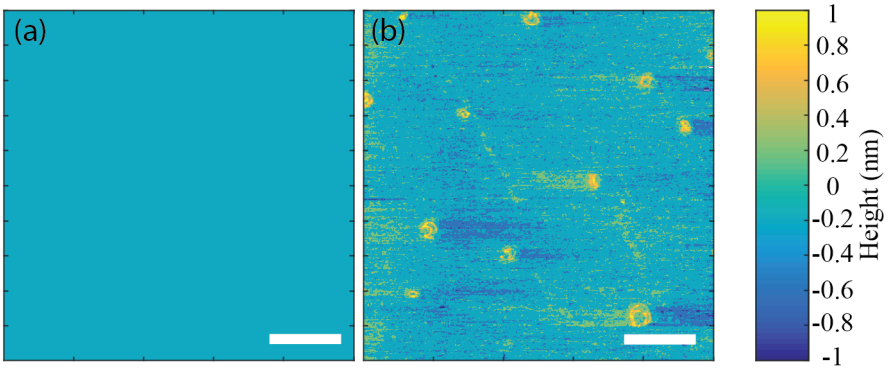

Figure S6 (a) Fluoro-silanized silicon wafer scanned in air at ambient conditions with an AFM. **(b)** The same region of interest scanned in milliQ water with an AFM. The scale bar is 1 μm.

Supplementary section 6: Investigation of planar and curved PPFS-modified surfaces

The same investigation, carried out with planar fluoro-silanized wafers, was also performed with planar PPFS-modified substrates. For these measurements, an OTS-modified AFM tip was used. Analogously to the fluoro-modified wafers, the PPFS-functionalized wafers present geometrical features which become more pronounced when the substrate is exposed to water (Figure S7). Despite being geometrically smooth overall, planar PPFS-modified surfaces may induce contact-line pinning due to local surface heterogeneities and therefore result in contact angle hysteresis. The latter is confirmed by the macroscopic contact angle measurements reported in **Table S4**.

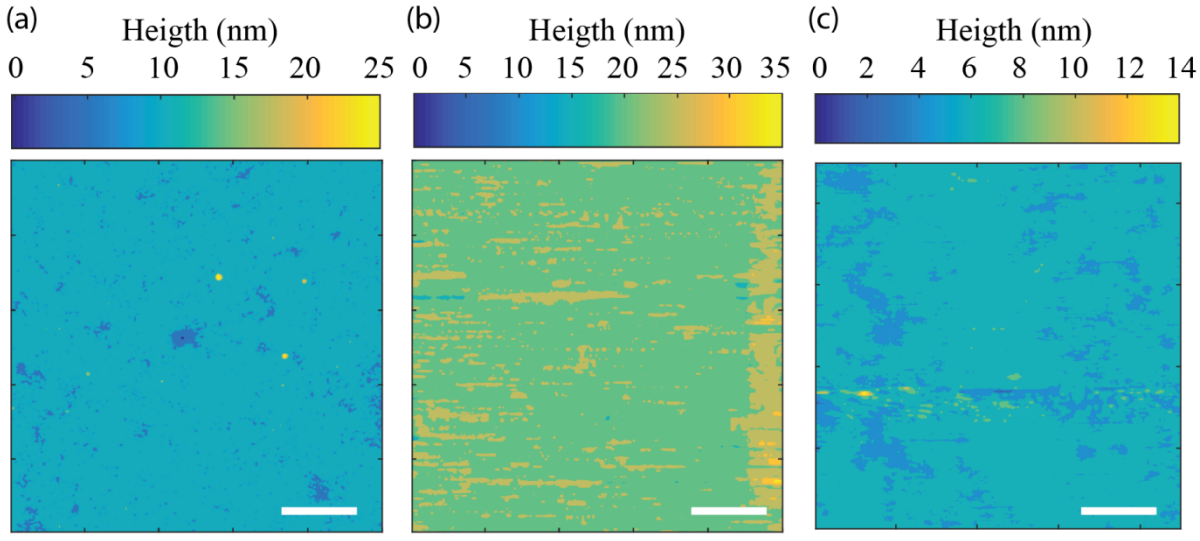

Figure S7 AFM scans of planar PPFS-modified silicon wafers. The measurements were carried out **(a)** in air at ambient conditions, **(b)** in water and **(c)** in n-hexadecane. The scale bar is 1 μm.

Table S4 Static ($\theta_s^{w/o}$), advancing ($\theta_a^{w/o}$) and receding ($\theta_r^{w/o}$) contact angles of water droplets placed on chemically modified silicon wafers immersed in n-hexadecane.

Functionalization	$\theta_s^{w/o}$(°)	$\theta_a^{w/o}$(°)	$\theta_r^{w/o}$(°)
PPFS	129 ± 1	132 ± 1	124 ± 1

The same line of thinking can be applied to PPFS-modified curved surfaces (colloidal spheres). Indeed, the SEM and AFM characterization (in air) of PPFS-functionalized colloids show a geometrically smooth surface (Figure S8). Nevertheless, these particles are able to impart quadrupolar deformations when adsorbed at liquid interfaces (see Figure 6 in the manuscript). All of the arguments presented above clearly indicate that the surface of fluorinated particles (either fluoro-silane, or PPFS) is chemically heterogeneous when exposed to water, thus able to pin the three-phase contact line.

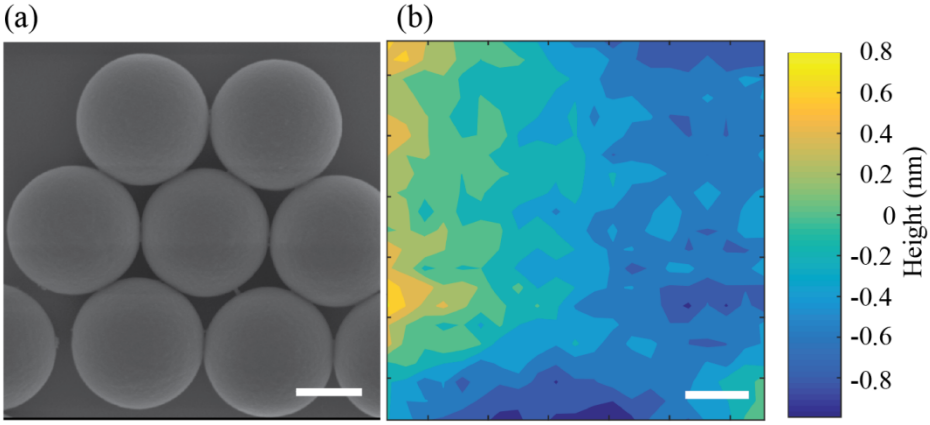

Figure S8 (a) SEM scan of PPFS-modified silica colloids and **(b)** Background-free AFM scan of a single PFFS functionalized particles in air. The scale bars are 500 nm in (a) and 50 nm in (b).

Supplementary section 7: Focused ion beam modification of a colloidal probe and its detachment characterization

The shape of one colloidal probe (R = 1.66 μm) was modified using a focused ion beam (FIB, Zeiss NVision 40) after it was glued to a tip-less AFM cantilever. A beam current of 10 pA with a dwell time of 102 μs was used to carve a circular groove along the particle surface. The cantilever was mounted in the FIB apparatus in such a way, so that the long side of the cantilever was perpendicular to the beam. The first half of the groove was produced by milling a 500-nm-wide and 200-nm-deep region. To complete the circular cut, the cantilever was removed from the FIB chamber and flipped along its longitudinal axis. The same milling procedure was then repeated on the other side of the particle. To compensate for the tilt of the

cantilever when mounted on the AFM stage, the cut was milled at a 10° angle with respect to the longitudinal axis of the cantilever.

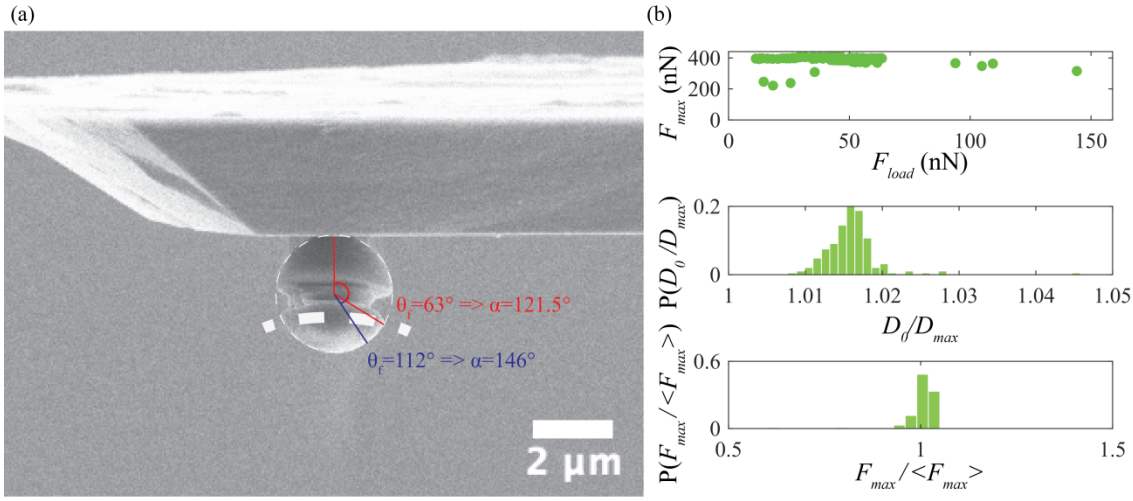

Figure S9 (a) SEM image of an FIB-cut colloidal probe (R = 1.66 µm). The cut (width of 500 nm and depth of 200 nm) is milled approximately around the equatorial position. The thick dashed line represents the position of the contact line at the moment of detachment. The thickness of the line corresponds to the standard deviation of the distribution of the detachment positions. The scale bar is 2 µm. **(b)** F_{max} as a function of the load F_{load} together with the histograms of D_0/D_{max} and $F_{max}/<F_{max}>$.

To further examine the pinning on fluorinated particles, we carried out force-distance measurements using the FIB-modified particle after fluoro-silanization on a water/n-hexadecane interface (see Figure **S9**). For all the exerted loads, the measured F_{max} is higher than the estimated F_{max} from Eq. 2 (see Figure S9b). In fact, assuming contact line sliding, a radius of 1.66 µm and a receding contact angle of 112°, F_{max} is estimated to be around 170 nN. This value is markedly lower than the measured $<F_{max}>$. From the mean value of the measured F_{max}, it is possible to calculate an apparent contact angle of 63° using Eq. 2 and thus the position at which the detachment takes place (α_{max} = 121.5°). The latter is highlighted in Figure S9a by the white dashed line, where the line thickness corresponds to the width of the distribution of F_{max} translated in terms of protrusion height. The nature and the geometry of the pinning position are believed to be responsible for the discrepancy between the measured and the expected force for contact line sliding. Additionally, it is further confirmed that Eq. 2 may lead to erroneous estimates when contact line pinning contributes to the detachment. Interestingly, for very few detachment curves, the measured F_{max} was lower in magnitude than $<F_{max}>$. These rare events could be due to incomplete pinning of the contact line at the edge of the groove. As previously discussed, for a perfect pinning-controlled detachment, D_{max} is equal to D_0. The fact that for the FIB-cut colloidal

probe D_0/D_{max} is not exactly equal to 1.00 suggests that the detachment events are not purely dominated by a fixed (pinned) contact line. Some relaxation of the contact line could happen because of the finite radius of the FIB-cut[6]. This defect may allow the contact line to slide for very short distances before experiencing an abrupt detachment.

Supplementary section 8: Ratio between D_0 and D_{max} for contact-line sliding

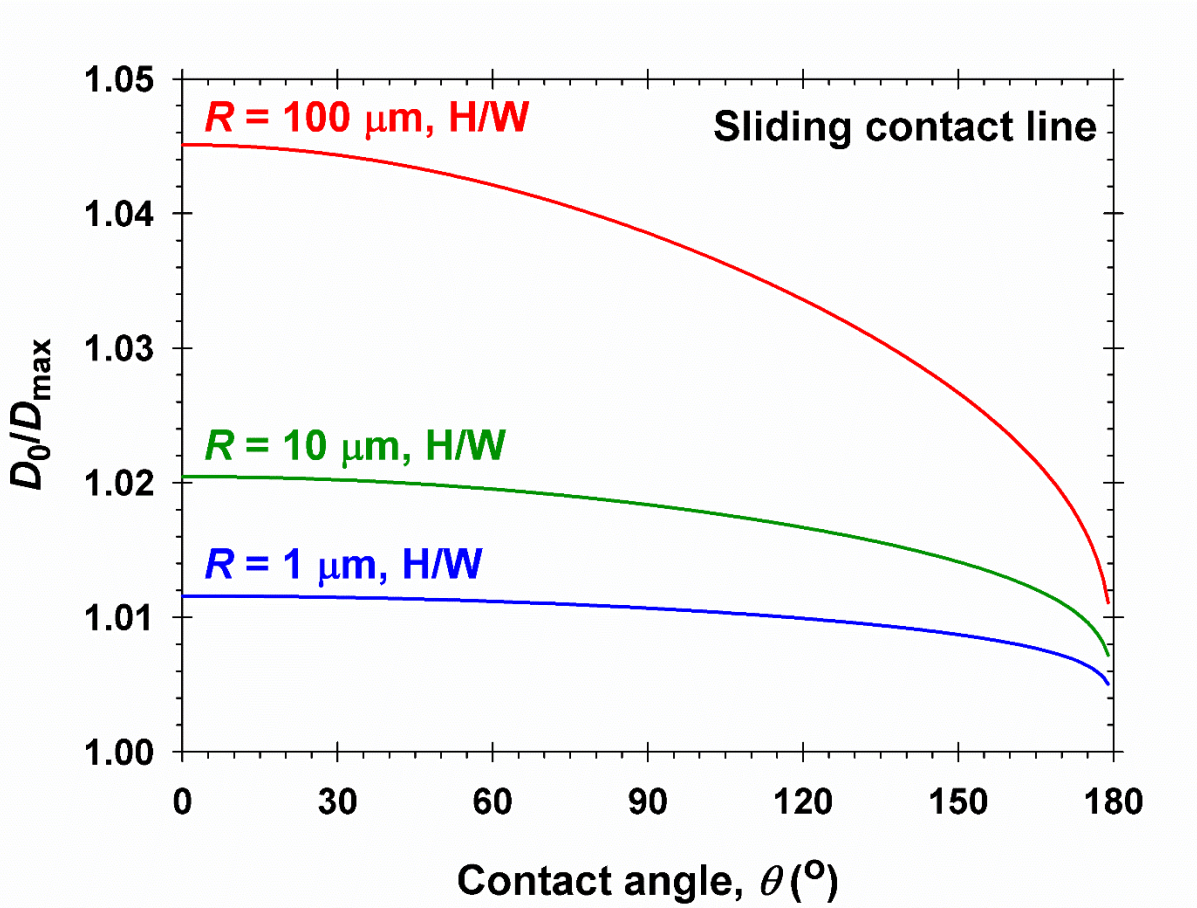

Figure S10 D_0/D_{max} is plotted as a function of the particle contact angle for sliding-controlled detachment from a water/n-hexadecane interface. All solid lines represent analytical calculations using the theory from Ref. 36 in the manuscript. The red line shows the trend for a colloidal probe with a diameter of 100 μm, the green line is for a colloidal probe with a diameter of 10 μm and the blue line is for a colloidal probe with a diameter of 1 μm.

Supplementary references

1. Isa, L.; Lucas, F.; Wepf, R.; Reimhult, E., Measuring single-nanoparticle wetting properties by freeze-fracture shadow-casting cryo-scanning electron microscopy. *Nat. Commun.* **2011,** *2*, 438.
2. Isa, L., Freeze-fracture Shadow-casting (FreSCa) Cryo-SEM as a Tool to Investigate the Wetting of Micro- and Nanoparticles at Liquid–Liquid Interfaces. *Chimia* **2013,** *67* (4), 231-235.
3. Paunov, V. N., Novel Method for Determining the Three-Phase Contact Angle of Colloid Particles Adsorbed at Air−Water and Oil−Water Interfaces. *Langmuir* **2003,** *19* (19), 7970-7976.
4. Zanini, M.; Marschelke, C.; Anachkov, S. E.; Marini, E.; Synytska, A.; Isa, L., Universal emulsion stabilization from the arrested adsorption of rough particles at liquid-liquid interfaces. *Nat. Commun.* **2017,** *8*, 15701.
5. Joanny, J. F.; de Gennes, P. G., A model for contact angle hysteresis. *J. Chem. Phys.* **1984,** *81* (1), 552-562.
6. Ally, J.; Kappl, M.; Butt, H.-J., Adhesion of Particles with Sharp Edges to Air–Liquid Interfaces. *Langmuir* **2012,** *28* (30), 11042-11047.